Reconciling single chamber Mg/Ca with whole shell $\delta^{18}O$ in surface to deep dwelling planktonic foraminifera from the Mozambique Channel

Juliane Steinhardt[1], Caroline Cléroux[1], Lennart de Nooijer[1], Geert-Jan Brummer[1,2], Rainer Zahn[4], Gerald Ganssen[2], Gert-Jan Reichart[1,3]

[1] *Department of Geology and Chemical Oceanography, NIOZ Royal Netherlands Institute for Sea Research, P.O. Box 59, NL-1790 AB Den Burg, Netherlands,* juliane.steinhardt@nioz.nl*

[2] *Faculty of Earth- and Life Sciences, VU University Amsterdam, de Boelelaan 1085, 1081 HV Amsterdam, The Netherlands*

[3] *Department of Earth Sciences, Faculty of Geosciences, Utrecht University, P.O. Box 80021, 3508TA Utrecht, The Netherlands*

[4] *Institució Catalana de Recerca i Estudis Avançats (ICREA) and Institut de Ciència i Tecnologia Ambientals, Departament de Física, Universitat Autònoma de Barcelona, Cerdanyola del Vallès, Spain.*

Corresponding author: juliane.steinhardt@nioz.nl

Abstract

Most planktonic foraminifera migrate vertically through the water column during life, meeting a range of depth-related conditions as they grow and calcify. For reconstructing past ocean conditions from geochemical signals recorded in their shells it is therefore necessary to know vertical habitat preferences. Species with a shallow habitat and limited vertical migration will reflect conditions of the surface mixed layer and short- and meso-scale (i.e. seasonal) perturbations therein. Species spanning a wider range of depth habitats, however, will contain a more heterogeneous, intra-specimen variability (e.g. Mg/Ca and $\delta^{18}O$), which is less for species calcifying below the thermocline. Obtained single-chamber Mg/Ca are combined with single specimen $\delta^{18}O$ and $\delta^{13}C$ of the surface water inhabitant *Globigerinoides ruber*, the thermocline-dwelling *Neogloboquadrina dutertrei* and *Pulleniatina obliquiloculata* and the deep dweller *Globorotalia scitula* from the Mozambique Channel. Species-specific Mg/Ca, $\delta^{13}C$ and $\delta^{18}O$ data combined with a depth-resolved mass balance model confirm distinctive migration and calcification patterns for each species as a function of hydrography. Whereas single specimen $\delta^{18}O$ not always reveal changes in depth habitat related to hydrography (e.g. temperature), measured Mg/Ca of the last chambers can only be explained by active migration in response to changes in temperature stratification. Foraminiferal geochemistry and modeled depth habitats shows that the single chamber Mg/Ca and single shell $\delta^{18}O$ are in agreement with each other and in line with the changes in hydrography induced by eddies.

1. Introduction

Most planktonic foraminifera inhabit the upper 200 meters of the water column, with exceptions of some species living as deep as 1000 m (e.g. Hemleben, 1989). The average depth habitat of individual species and the range of water depths at which they are found reflect their ecology (e.g. feeding behavior), ontogeny and seasonal preferences. Stable oxygen isotope values ($\delta^{18}O$) and Mg/Ca ratios (Shackleton et al., 1974; Fairbanks et al., 1980; Ortiz et al., 1996; Elderfield and Ganssen, 2000) have been used to reconstruct upper water column conditions using species with a known depth range (e.g. Ravelo et al., 1992; Patrick and Thunell, 1997; Faul et al., 2000; Cléroux et al., 2013). For many species, however, application of Mg/Ca as a seawater temperature proxy is complicated by depth migration as a function of ontogeny. Previous studies revealed major Mg/Ca heterogeneity within foraminiferal shells (e.g. Eggins et al., 2003; Hathorne et al., 2009; Kunioka et al., 2006; Jonkers et al., 2012), which were attributed to a combination of vertical migration during their life and vital effects. Nevertheless, species-specific patterns of vertical migration and hence depth of calcification determine which part of the water column can be reconstructed.

Field observations show that most foraminiferal species do not occupy a single depth, but rather calcify at a range of depths. Many species migrate vertically as they grow and, therefore, the chemical composition (e.g. Mg/Ca and $\delta^{18}O$) of their shells changes with age. Fairbanks et al. (1982) and Field (2004) suggested that foraminifera may modify their habitat depth depending on hydrographic condition and food supply. However, little is known about the exact controls on depth habitat, termination of shell growth and controls on shell features (e.g. formation of crusts). A better understanding of the vertical calcification pattern of different species is needed to reconstruct past changes in vertical structure of the water column by using geochemical proxies, e.g. for temperature ($\delta^{18}O$ and Mg/Ca). Using geochemical signals of species with different and well-constrained calcification depths (Emiliani, 1954; Mulitza et al., 1997) changes in water column conditions can be resolved.

Using core top samples from the Indian Ocean, Birch et al. (2013) report $\delta^{13}C$ and $\delta^{18}O$ measurements made on several species of planktonic foraminifera across a range of tightly constrained size windows. From size controlled $\delta^{18}O$ calcite trajectories they inferred depth habitats, using modern vertical temperature profiles. However, by using multiple core-top specimens this data set encompasses not only vertical changes in the water column structure, but also inter- and intra-annual changes therein, which are both known to vary substantially in this region (e.g. McClanahan, 1988; Damassa et al., 2006; Hastenrath et al., 1993). In this study we

use sediment trap samples, allowing analyses of specimens that lived during a confined time interval and link in situ hydrographic changes (i.e. temperature) more directly to their shell chemistry.

Single-chamber Mg/Ca compositions from specimens with contrasting calcification depths (the surface-dweller *Globigerinoides ruber* (d' Orbigny, 1839), the thermocline-dwelling species *Neogloboquadrina dutertrei* (d' Orbigny, 1839) and *Pulleniatina obliquiloculata* (Parker et al., 1865) and the deep dweller *Globorotalia scitula* (Brady, 1882) reflect temperatures throughout the upper 500 m and were shown to reliably reflect short-term hydrographic changes (Steinhardt et al., 2014). Meso-scale eddies such as observed in the Mozambique Channel (MC) induce variations in temperature and salinity. Anticyclonic (anti-clockwise) eddies in the MC are characterized by a warm water core and are associated with elevated sea surface heights and large vertical isopycnal excursions. Foraminifera living in the mixed layer of the MC are affected by eddy-induced changes, which is reflected by the geochemistry of *G. ruber* and *N. dutertrei* (Steinhardt et al., 2014), resulting in higher Mg/Ca ratios and more depleted $\delta^{18}O_{cc}$ values. These short-term changes in vertical water column temperature and $\delta^{18}O_{sw}$ distribution should influence shell $\delta^{18}O$ and Mg/Ca throughout the different ontogenetic stages for any species migrating during its life. Alternatively, foraminifera may respond to altered hydrographic conditions by changing their calcification depth. Here we present combined single-specimen $\delta^{18}O$ and single-chamber Mg/Ca measurements for different species, providing a composite of thermocline and sub-thermocline conditions. Since single chamber Mg/Ca values cannot be compared one-on-one with whole shell $\delta^{18}O$-values we evaluate our results using a mass balance model for depth related carbonate addition of four species of planktonic foraminifera.

2. Oceanographic setting

In the oligotrophic Mozambique Channel (MC) (Fig. 1) sea surface temperatures (SST) vary seasonally and with eddy-induced transport (Fallet et al., 2011). The SSTs range from 25°C to over 30°C with an annual mean of 27.6°C, the seasonal change in temperatures is associated with the monsoon system. With the onset of Austral summer rainfall increases, caused by the seasonal migration of the ITCZ and sea surface salinities decrease slightly from 35.2 in winter to 34.9 in summer (Fallet et al., 2010). Depth of the calcite compensation in the Western Indian Ocean is below 3000 meters and hence promotes preservation of foraminiferal calcite at the seafloor of the Mozambique Channel that has a depth of 2225 m at the trap location. Southward migration of anticyclonic meso-scale eddies, originating at 10°S north off the Comoros Islands,

affects the hydrography in the MC (Fig. 1). Eddies pass through the MC at a mean frequency of about four to seven per year (at a southward propagation speed of 3-6 km.d^{-1}) before joining the Agulhas Current. An eddy passage is associated with vertical movement of isopycnals, which can occasionally exceed 40 m per day in the upper layer (Ullgren et al., 2012). The formation of meso-scale eddies in the Mozambique Channel is related to variability in the South Equatorial Current (SEC) transport (Backeberg and Reason, 2010) (Fig. 1). The main water masses contributing to the upper part of the MC include the Tropical Surface Water (TSW), Subtropical Surface Water (STSW) and Indonesian Throughflow Water (ITFW). The warm, fresh surface water (TSW) forms in the tropics and is transported westward within or north of the SEC (New et al., 2007). In the proximity of the western margin, where the SEC bifurcates, warm surface waters are transported poleward, either east of Madagascar, or through the MC (e.g. Gründlingh, 1995; Swallow et al., 1988). The STSW is characterized by relatively high salinities and a subsurface maximum, with salinities of 35.2 – 35.5, at approximately 200 m below sea surface, at which depth the surface water subducts below the fresher TSW (Wyrtki, 1973).

3. Material & Methods

3.1 Sediment trap and mooring array

Within the Long-term Ocean Climate Observations (LOCO) program, an array of eight moorings across the narrowest part of the Mozambique Channel, provides continuous measurements of current velocities, temperatures and salinities at fixed depths since November 2003 (Ullgren et al., 2012). Sediment traps of the type Technicap PPS 5 were deployed at 16.8°S and 40.8°E in the central MC (Fig. 1), equipped with an automated sampling carousel of 24 cups and a baffled collecting area of 1 m^2. The trap was positioned 250 m above the channel floor at 2250 m water depth. Between November 2003 and February 2009, a total of four sediment trap deployments took place, each programmed to a 17, 21 or 23 days sampling interval. Prior to deployments, sample cups were filled with an $HgCl_2$-poisoned and borax-buffered solution of seawater collected from the deployments depth (Lončarić et al., 2007). Sediment trap samples were wet-split, sieved and foraminiferal shells were cleaned according to the protocol of Barker et al. (2003), modified after Fallet et al. (2009) (Fallet et al., 2010; Steinhardt et al., 2014).

Using sediment trap material allows to link the chemistry of the shells to actual ambient *in situ* measurements from the moorings and from real-time satellite derived observations. Therefore we are able to link short time changes in hydrography (i.e. eddies) to the differences in shell chemistry. Calculated back trajectories, based on a high-resolution INALT01 model (Durgadoo, 2013), show that specimens ending up in the sediment trap all originate from the area under influence of the

eddy-variability (Steinhardt et al., 2014). We selected the sediment trap intervals during which the complete sediment cup collection took place under either full eddy or full non-eddy conditions (for full description see Steinhardt et al., 2014; supplement). For the selected collecting intervals, temperature and salinity observations from the mooring (lmc5a) are compiled and daily means were used to calculate eddy and non-eddy temperature profiles.

3.2 Temperature and Salinity data

For this study, we used temperatures recorded at 110 m; 200 m and 400 m water depth by a CTD deployed on mooring lmc5A (16.8°S, 41.1°E, Fig. 1), which is closest to the sediment trap site. Moored salinity and temperature data, collected during the selected intervals of eddy and non-eddy conditions (Table S1 in the Supplement), was spline fitted in Analyseries 1.1.6 68K to achieve meter-wise data resolution. Sea surface temperatures were retrieved from the 4 km daytime MODIS/AQUA dataset around trap site (16 – 17°S and 40 – 41°E) for the period of the selected collecting intervals (http://poet.jpl.nasa.gov/). Surface salinity data is not available for the complete deployment period and instead, CTD-based salinity-depth profiles taken during the deployment/recovery cruises were used (Ullgren et al., 2012). Based on the trend observed in the moored salinity data at 110 m water depth (Ullgren et al., 2012; less saline during eddy condition) we use CTD minimum surface salinities to represent eddy surface salinities and maximum surface salinities to represent non-eddy conditions. Since salinity mooring data was non-existent between 400 and 1525 m, we have chosen two more "anchor points" at 700 and 1000 m water depth from the CTD depth profiles in order to better capture the Red Sea Water (RSW) advection at these depths and to achieve a more accurate salinity fitting curve for the upper 1000 m.

3.3 Planktonic foraminiferal species and ontogeny

We selected four species from the sediment trap samples according to differences in depth habitats as reported in previous studies. *Globigerinoides ruber* (white) is a shallow, surface mixed layer dwelling species, occupying the upper 50 m of the water column and is commonly used to reconstruct paleo-SST (Hemleben et al., 1989). To minimize a potential biases in $\delta^{18}O$ and Mg/Ca associated when combining different morphotypes (Steinke et al., 2005), we used only *G. ruber* sensu stricto that was by far the most abundant in these samples (Fallet et al., 2010).

The subsurface-dwellers *Neogloboquadrina dutertrei* and *Pulleniatina obliquiloculata* have been associated with a calcification depth of 0 - 100 meters and 60 - 150 meters in the upper and middle thermocline, respectively (Erez and Honjo, 1981; Fairbanks et al., 1982; Ravelo and Fairbanks, 1992; Spero et al., 2003; Field, 2004; Kuroyanagi and Kawahata, 2004; Huang et al., 2008). The

deep-dwelling species *Globorotalia scitula* was used as a representative for deep water conditions (Bé, 1969; Ortiz et al., 1996; Itou et al., 2001; Fallet et al., 2011).

Measurements on *G. ruber* were usually performed on specimens in the 250 - 315 µm size fraction. In a limited number of samples, abundances of this species were low in this size fraction, and geochemical analyses were therefore performed on specimens from a larger size fraction (315 - 400 µm). Analyses on *N. dutertrei*, *P. obliquiloculata* and *G. scitula* were generally done on the size range >315 µm, with additional measurements on the 250 - 315 µm size fraction depending on the specimen's abundance within a sample. All specimens show excellent preservation and do not show any signs of diagenesis (based on SEM microscopy). Recently, Fallet et al. (2012) showed that shell size normalized weights of three species of planktonic foraminifera from the same sediment trap location do not differ from those of the surface sediment samples below this trap. Absence of dissolution is also reported by Birch et al. (2013) describing planktonic foraminifera from surface sediments at ~ 3000 m water depth, in the northern part of the Mozambique Channel, as being glassy and preserved excellently.

3.4 Mg/Ca and Stable isotope analyses

The Mg/Ca ratios of single chambers used in this study were previously published (Steinhardt et al., 2014) and were determined by Laser Ablation-Inductively Coupled Plasma-Mass Spectrometry (LA-ICP-MS) at Utrecht University (Reichart et al., 2003) (for summary of the results see Tab. 1). Subsequently, specimens were analyzed for whole shell $\delta^{18}O$ and $\delta^{13}C$ after microscopic removal from the laser ablation stub with ethanol and inspection for possible contaminations. Measurements were performed at the Universitat Autònoma de Barcelona on a Thermo Finnigan MAT253 mass spectrometer coupled to a Kiel IV device for CO_2 sample gas preparation. External reproducibility (1σ) of $\delta^{13}C$ standards NBS19 and IAEA-CO was 0.04‰ and for $\delta^{18}O$ 0.08‰.

Single shells from part of the sample set were analyzed using a Thermo Finnigan Delta Plus mass spectrometer equipped with a Gas Bench II preparation device at the VU University Amsterdam. Single specimens were loaded into round-bottom vials, which were subsequently flushed with He. The samples then reacted with phosphoric acid (H_3PO_4) injected into the vial producing CO_2 gas, which is transported in a helium stream to the mass spectrometer. Traps are used to remove residual H_2O from the sample gas and the CO_2 is separated from other possible contaminant gases on a poraplot Q GC column. Reproducibility (1σ) of $\delta^{13}C$ standards NBS19 and was 0.07‰ and for $\delta^{18}O$ 0.12‰. Values measured on the Kiel IV and the GASBENCH-II are comparable and species-specific $\delta^{18}O_{CC}$ are in good agreement (Tab. 2). Measurements with the GASBENCH-II

have a somewhat wider standard deviation inherent to continuous flow mass spectrometry. In total, 391 single shell stable isotope values were obtained. Values deviating more than twice the standard deviation from the average of the total dataset were regarded as outliers (n=23) and removed from the dataset (Tab. S3).

The $\delta^{18}O_{sw}$, expressed on the SMOW scale is converted to Pee Dee Belemnite (PDB) scale by subtracting 0.27‰ (Hut, 1987). Various $\delta^{18}O$-temperature equations have been proposed and discussed in detail in other studies (Bemis et al., 1998; Regenberg et al., 2009), without clear consensus on the most appropriate equation. Here, we integrated calcification depth for each species calculated by matching the foraminiferal calcite $\delta^{18}O_{CC}$ with the calculated calcite $\delta^{18}O_{calc}$ following equation (1) from Kim and O'Neil (1997) for the temperature dependent fractionation of calcite by inorganic precipitation (assuming calcification in equilibrium with the ambient seawater).

(1) $\delta^{18}O_{eq} = 25.778 - 3.333 \times \sqrt{43.704 + T} + (\delta^{18}O_{sw} - 0.27)$

We extracted $\delta^{18}O_{sw}$ values from the South Indian Ocean for the upper 2000 m (4.5 - 120.2°E; 0 - 32.9°S, N=154) from the Global Seawater Oxygen-18 Database (see supplementary table, http://data.giss.nasa.gov/o18data/). Additionally we included in situ $\delta^{18}O_{sw}$ measurements from the MC, near the sediment trap location (41.08°E; 16.74°S) in order to determine the regional relationship between $\delta^{18}O_{sw}$ and salinity (Eq. 2)

(2) $S = 0.463 * \delta^{18}O_{sw} - 15.9$, $r^2 = 0.87$

This linear relationship (3) is subsequently used to estimate $\delta^{18}O_{sw}$ values based on salinities measured in the proximity of the trap by moored T-S sensors during eddy and non-eddy conditions for depths ranging from 0 to 1000 m.

Seawater temperature and estimated $\delta^{18}O_{sw}$ profiles for eddy or non-eddy conditions are used to compare the $\delta^{18}O$ data depending on the time interval sampled by the sediment trap. We used averaged $\delta^{18}O_{sw}$ from the depth range suggested by previously measured single chamber Mg/Ca analyses (Steinhardt et al., 2014), to calculate the $\delta^{18}O$-derived calcification temperature for all species, following the temperature equation of Kim and O'Neil (1997):

(3) $T = 16.1 - 4.64*(\delta^{18}O_{CC} - (\delta^{18}O_{SW}-0.27)) + 0.09*(\delta^{18}O_{CC} - (\delta^{18}O_{SW}-0.27))^2$

238 The temperature equation of Kim an O'Neil (1997) is the most general calibration, which allows
239 comparing inter specific differences that are automatically accounted for when using species-
240 specific calibrations.
241
242 ## 4. Results
243 ### 4.1 Oxygen isotopes
244 Single specimen values of $\delta^{18}O_{CC}$ range from -3.50‰ to 2.65‰. Although the values measured
245 on individual specimens clearly overlap, each species has a different average $\delta^{18}O_{CC}$ and $\delta^{13}C_{CC}$
246 (Fig. 2 and 3). The $\delta^{18}O_{CC}$ values are most depleted for *G. ruber*, somewhat more enriched in
247 comparison to *G. ruber* for *P. obliquiloculata* and *N. dutertrei,* with most enriched values in *G.*
248 *scitula* (Tab. 1, Fig. 2 and 3). The relationship between temperature and $\delta^{18}O_{CC}$ is generally
249 described with more depleted $\delta^{18}O_{CC}$ values indicating higher temperatures and thereby shallower
250 calcification depths. Thus, each species has a distinct whole shell-$\delta^{18}O$ signature, reflecting their
251 different mean calcification depth*. G. ruber* (-2.57±0.04‰*,* SD: ±0.24‰), *N. dutertrei* and *P.*
252 *obliquiloculata* record negative $\delta^{18}O_{CC}$ values between -1.53±0.03‰ (standard deviation (SD): ±0.
253 42‰) and -1.13± 0.04‰ (SD: ±0.24‰), more noticeable positive values are found for *G. scitula*
254 with 1.47± 0.14‰ (SD: ±0.87‰) (Fig. 3). No significant trend between size fractions and stable
255 isotopes was observed for any of the analyzed species over the size range we used, as confirmed
256 by ANOVA tests (Kruskal-Wallis one way analysis of variance on ranks) of $\delta^{18}O_{cc}$ between the
257 size fractions (*G. ruber*: p= 0.774, *N. dutertrei*: p= 0.500, *G. scitula*: p= 0.373).

258 No significant differences in $\delta^{18}O$ values for *G. ruber* and *N. dutertrei* were found between eddy
259 and non-eddy conditions. In the deeper dwelling species *P. obliquiloculata* (U=54, P=0.04) and *G.*
260 *scitula* (U=80, P=0.021), most depleted $\delta^{18}O$ values were found during eddy conditions and non-
261 eddy conditions, respectively (Tab. 3; Fig. 3).
262
263 ### 4.2 Carbon isotopes
264 Values for $\delta^{13}C$ range from -1.5‰ to 2.0‰. Most enriched $\delta^{13}C$ values are found in *N. dutertrei*
265 ($\delta^{13}C$= 0.53±0.042‰, SD: ±0.44‰), whereas values for *P. obliquiloculata* are most depleted
266 ($\delta^{13}C$= 0.04±0.04‰, SD: ±0.21‰). Individuals of *G. ruber* reflect a relatively large range in $\delta^{13}C_{cc}$
267 values (0.51±0.04‰, SD: ±0.47‰), whereas *G. scitula* (0.27±0.04‰, SD: ±0.22‰) displays a
268 much more limited variability in $\delta^{13}C_{CC}$ (Tab. 1, Fig. 3). Species specific $\delta^{13}C$ - $\delta^{18}O$ relationships
269 (Fig. 2) differ and only *G. scitula* showed a positive correlation between single specimen carbon
270 and oxygen isotope ratios (Fig. 2, r^2=0.388, p<0.001). Moreover, values for *G. scitula* differ from

those of other species, with relatively depleted $\delta^{13}C$ (0.27‰, SD: ±0.22‰) and relatively enriched $\delta^{18}O$ values (1.47‰, SD: ±0.87‰).

From the four investigated species, only *G. scitula (*N: 37) did not show a significant difference in $\delta^{13}C$ between eddy and non-eddy conditions. *G. ruber* (N: 200; Mann-Whitney rank sum test U= 3373, p = 0.002), and *P. obliquiloculata* (N: 33; U= 52, p = 0.032) showed significantly more positive $\delta^{13}C$ values during non-eddy conditions. During non-eddy condition however, *N. dutertrei* (N: 118; U= 939.5, p = 0.002) recorded more negative $\delta^{13}C$ values (Fig. 3).

4.3 Calcification temperatures

The calculated multi-specimen $\delta^{18}O$-based temperature from eq. (3) and the single chamber Mg/Ca are positively, exponentially correlated (Fig. 4). Variability in this relationship is highest at higher (> 25°C) temperatures. Mg/Ca-derived calcification temperatures, for *G. ruber* are on average 28.1±2.8°C, based on the calibration of Fallet et al. (2010) for this species in this region. Calcification temperatures for *N. dutertrei* and *P. obliquiloculata* are 22.5±3.7°C and 21.6±3.1ºC, respectively, both based on species-specific calibrations from Anand et al. (2003). Mg/Ca ratios of *G. scitula* were transformed into temperatures using the equation for *G. hirsuta* (Anand et al., 2003) resulting in an average temperature of 14.4±3.4°C (Fig. 5). Calcification temperatures based on $\delta^{18}O$ result in markedly different values, ranging from 29.4±1.3°C for *G. ruber* to 24.4±2°C for *N. dutertrei*, 22.5±1.1°C, for *P. obliquiloculata* and 10.4±3.9°C for *G. scitula* (Tab. 1). Since *P. obliquiloculata* and *G. scitula* showed significant differences for $\delta^{18}O_{CC}$ between eddy and non-eddy conditions, we separately calculated temperatures for eddy and non-eddy condition. Mean $\delta^{18}O$ from Eq. (3) for eddy intervals yield 22.8±0.9°C for *P. obliquiloculata* and 7.9±2.1°C for *G. scitula*. For non-eddy intervals calcification temperatures are 22.5±1.2°C for *P. obliquiloculata* and 11.8±4.1°C for *G. scitula* (Fig. 5).

5. Discussion:

5.1 Single specimen isotope temperatures

The average, single-specimen $\delta^{18}O_{CC}$ of *G. ruber* reflect SSTs of 27.0±2.2°C - 28.4±2.1°C (based on sediment-trap calibrations from Fallet et al., 2010 and Wilke et al., 2009, respectively), which is close to the satellite-derived annual mean SST of 27.6°C (Fallet et al., 2010). When applying the equation of Kim and O'Neil (1997) for conversion of $\delta^{18}O_{CC}$ into temperature SST is considerably higher (29.4±1.3°C). This discrepancy, may be caused by the fact that the calcite-water calibration of Kim and O'Neil (1997) is based on inorganic precipitation experiments, free of

vital effects and therefore may be offset compared to the temperature-$\delta^{18}O_{CC}$ relationship of biogenic carbonates. Nevertheless this temperature estimate based on Kim and O'Neil (1997) is in good agreement with the average temperature of 28±1.1°C during the investigated intervals. The intertest variability of this species can be explained by the high temperature variability at the sea surface, as well as differences in symbiont activity. The shallow depth habitat of *G. ruber* in the MC is in line with previous studies showing that this species is confined to the photic zone (e.g. Deuser et al*.,* 1981*;* Lončarić et al*.,* 2006*;* Peeters and Brummer*,* 2002), because of the light requirement of its symbionts. Based on its relatively narrow preferred depth habitat, this species is a suitable tracer for (sub)tropical surface-water (0 - 100 meters, mixed layer) conditions (e.g. Deuser, 1987; Anand et al., 2003; Field, 2004; Fallet et al., 2010). Birch at al. (2013) show that shell size of specimens of *G. ruber* is not correlated to δ^{18}Occ, confirming that this species occupies a narrow calcification depth during its life. In addition to its shallow living depth, *G. ruber* is known to occur in some areas relatively equally throughout the year (e.g. Deuser, 1987; Mohtadi et al., 2006; Tedesco et al., 2007), whereas in other areas, including the MC, they occur at highest densities during summer months (e.g. Tolderlund and Bé, 1971; Duplessy et al., 1981; Ganssen and Sarnthein, 1983; Deuser and Ross, 1989; Eguchi et al., 2003; Lončarić et al., 2006; Fallet et al., 2010). This seasonal preference results in SSTs that are slightly biased towards summer conditions when using fossil specimens of this species.

Based on an average $\delta^{18}O_{CC}$-derived temperature of 24.3±2°C (Tab. 2), following the equation of Kim and O'Neil (1997), calcification depths of *N. dutertrei* are in the range of 20 - 130 m (Fig. 6) with an average of 58 m. For eddy conditions, the average calcification depth is approximately 80 m, for non-eddy condition it is approximately 37 m. Average Mg/Ca-based temperature of 22.5±4°C is in relatively good agreement with the average $\delta^{18}O_{CC}$-derived temperature (Tab. 2). The difference between Mg/Ca- and δ^{18}O-based temperatures are smaller than the 1.2°C uncertainty associate with the Mg/Ca calibration (Anand et al., 2003). Previous studies using *N. dutertrei* from Indian Ocean core top samples and Mozambique Channel sediment traps have reported similar depth ranges between 40 - 150 m (Kiefer et al., 2006) and similar average depths of 80 m (Fallet et al., 2011), respectively. Both of these studies used pooled specimen for their stable isotope analysis and hence provided the population's average calcification depth. Moreover, pooling of specimens from sediment core samples (Kiefer et al., 2006) does not allow for resolving short-term variability in calcification temperatures as do single specimens (e.g. seasonality). The inferred calcification depth for *N. dutertrei* is in line with its characterization as an intermediate deep dwelling species, living preferentially in the seasonal thermocline (e.g.

Fairbanks et al., 1982; Curry et al., 1983; Eguchi et al., 2003; Farmer et al., 2007), coinciding with a deep chlorophyll maximum (Fairbanks et al., 1980; Ravelo et al., 1990). Overall living depth of this species is confined to the upper 200 m (Farmer et al., 2007; Kroon and Darling, 1995). Variability in Mg/Ca within single specimen shell walls of *N. dutertrei* from the Timor Sea suggested temperatures between 12 and 23°C, implying migration through the entire thermocline (Eggins et al., 2003). However, most calcification seems limited to a much smaller depth interval and the extremes in Mg/Ca might reflect upper and lower depth limits occupied by this species. Moreover, banding of Mg/Ca in shell calcite has been viewed in terms of discrete calcification events (Elderfield et al., 1996; Erez et al., 2003). Plankton tow studies (Fairbanks et al., 1980) showed oxygen isotope equilibrium calcification for *N. dutertrei* and *P. obliquiloculata*.

The $\delta^{18}O_{CC}$-based calcification depths for *P. obliquiloculata* reported here (48-125 m, with an average of 74 m, Fig. 6) are in close agreement with those reported previously (e.g. between 60 and 80 m; Mohtadi et al., 2009). Indeed, in plankton tows from the central equatorial Pacific the largest abundance of adult *P. obliquiloculata* with a terminal cortex was found below 60 m (Watkins et al., 1996). All specimens used in this study had the distinctive smooth outer cortex that envelops the final whorl in the adult as well as an arched aperture (Watkins et al., 1996). Non-corticated *P. obliquiloculata* ("juveniles") are confined mostly to the mixed layer (Watkins et al., 1996), indicating migration to greater depths at the time of cortex formation during the terminal stage of its life cycle (Erez and Honjo, 1981; Hemleben et al., 1989; Ravelo and Fairbanks, 1992).

The average $\delta^{18}O_{CC}$ for *G. scitula* yields a calcification temperature of 10.4±3.9°C, suggesting that this species calcifies between 290 and 1100 m (Fig. 6) with an average of approximately 500 m. This overlaps with the depth rage indicated by the Mg/Ca temperatures of 14.4±3.4°C derived from the last few chambers added, suggesting that these shells formed at a depth between about 250 and 350 meter for non-eddy and eddy conditions respectively. The $\delta^{18}O_{cc}$ based estimates, however, do not consider possible vital effects that were previously suggested for this species (e.g. Kahn and Williams, 1981). If taken into account, this would lower the temperature and depth habitat estimates by some 4°C and 500 m, respectively.

Birch et al. (2013) support previous findings of a distinct positive correlation between $\delta^{18}O$ and size in *G. scitula* (e.g. Friedrich et al., 2012), which is linked to a substantial ontogenetic vertical migration through the water column. Largest individuals have been inferred to live below the thermocline, consistent with the supposed absence of symbionts in this species. This is in line with our observations, showing higher inter-specimen variability in $\delta^{18}O_{CC}$ for *G. scitula*, than in the other species.

372

373 **5.2 Habitat depth versus calcification depth**

374 Planktonic foraminifera collected by sediment traps might record $\delta^{18}O_{cc}$ signals comprising
375 calcification at various depths and thus document an *apparent* average calcification depth by
376 integrating the entire calcification history of the specimen. Given changes in seawater temperature
377 with water depth, even minor changes in the upper or lower range of the depth at which planktonic
378 species calcify, can have a profound effect on the average $\delta^{18}O_{cc}$ and reconstructed temperature.
379 Since evidence is accumulating that some species have a flexible calcification range (e.g. due to
380 seasonality or local hydrography; Lončarić et al., 2006; Wilke et al., 2009), interpretation of down
381 core stable isotope data in terms of thermal structure may be challenging. Therefore, it is crucial
382 to accurately quantify the impact of environmental factors on depth preferences of planktonic
383 foraminifera. Contrasting eddy and non-eddy conditions, a short-term feature, allow us to
384 disentangle seasonal and other short-term local hydrography changes and their effect on
385 foraminiferal calcification depth.
386 While Mg/Ca-based temperatures of *G. ruber* and *N. dutertrei* record eddy induced changes in
387 upper water column stratification (Steinhardt et al., 2014), $\delta^{18}O$-based temperatures are relatively
388 similar for both species (Fig. 6). Using the paleo-temperature equation (equation (1); Kim and
389 O'Neil, 1997) and fitting $\delta^{18}O_{calc}$ with $\delta^{18}O_{cc}$, we find that *G. ruber* calcifies on average at the sea
390 surface (down to 7 m during non-eddy conditions and down to 18 m under eddy conditions) (Fig.
391 6). *N. dutertrei* calcifies on average between 12 and 120 m during eddy conditions (average
392 calcification depth 81 m) and between 17 and 58 m under non-eddy conditions (average 37 m).
393 During eddy conditions, *P. obliquiloculata* calcifies between 89 and 124 m (average 107 m),
394 whereas it calcifies at shallower depth, between 20 and 77 m (average calcification depth 60 m)
395 during non-eddy condition. Largest changes in calcification depth in this study are inferred from
396 *G. scitula*. From a calcification range between 500 to 1100 m and an average calcification around
397 716 m during eddy condition it shifts to a calcification range from 168 to 745 m and an average
398 calcification depth of 343 m (Fig. 6).
399
400 Conversely, $\delta^{18}O$-based temperatures are significantly different for *P. obliquiloculata* and *G.*
401 *scitula*, while the Mg/Ca-based temperature of the last formed chambers of *P. obliquiloculata*
402 indicate similar calcification temperature (Tab. 1). Mg/Ca inferred calcification temperatures,
403 representing the depth occupied at the later stages of the foraminifer's life, were similar between
404 eddy and non-eddy conditions. Nonetheless, temperature mooring data show a steep temperature
405 gradient, coinciding with the habitat depth of *G. scitula,* and thereby revealing a wide range of

406 calcification depths for this species, changing significantly with deepening of the thermocline
407 during eddy passage.
408
409 Inferred higher variability in calcification temperature for *G. ruber* presented in this study compared
410 to observed satellite SST likely results from the spatial resolution employed here. Inter-individual
411 differences in depth migration add to the variability in isotopes and element/Ca ratios when
412 measuring single specimens. Potential effects of ontogeny on stable isotope composition are
413 minimized by using narrow size fractions, as confirmed by the lack of ontogenetic trends with shell
414 size in our measurements. Russell and Spero (2000) concluded that natural variability in oxygen
415 isotopes is species specific. Measuring single specimen $\delta^{18}O_{cc}$ of *G. ruber* shells from sediment
416 traps in the eastern equatorial Pacific, they show that over a 1.5 – 3 day period, the standard
417 deviation of $\delta^{18}O$ results in a temperature variability of ±0.87ºC. Such a variability could explain
418 between 12 and 38% of the variability in $\delta^{18}O$-based temperatures in our samples. Another cause
419 of natural variability might be differences in depth at which an individual calcifies. In laboratory
420 cultures, the addition rate of new chambers in *G. sacculifer* ranges from 1.6 to 6.2 days (Bé, 1981),
421 while chamber formation in *G. hirsuta* and *G. truncatulinoides* takes about 5 to 6 hours (Bé, 1979).
422 Considering that our sample duration ranges between 17 and 21 days, $\delta^{18}O$ variability is likely to
423 be affected by other parameters (e.g. temperature). Therefore, the observed variability in $\delta^{18}O$-
424 based temperatures caused by species specific natural variability in $\delta^{18}O_{CC}$ (e.g. Russell and
425 Spero, 2000) during the time it takes to add new chambers, which might be calcified under different
426 conditions or water depth.
427
428 **5.3 Reconciling $\delta^{18}O$ and Mg/Ca-derived calcification depths**
429 Mg/Ca-derived temperatures indicate that calcification depths of *N. dutertrei* range between 42-
430 169 m (average depth: 81 m) under non-eddy conditions and between 13 and 196 m (average
431 depth: 98 m) during eddy conditions (Steinhardt et al., 2014). Thus, the shoaling in average
432 calcification depth from 98 m during eddy conditions to 81 m during non-eddy conditions, indicated
433 by the whole shell $\delta^{18}O_{cc}$ is less as than inferred from Mg/Ca, derived from the calcification of the
434 last chambers. A more pronounced trend is present in Mg/Ca of *P. obliquiloculata,* shifting
435 between 70 and 90 m (average 75 m) during non-eddy conditions, to depths between 147 and
436 244 m (average 150 m) during eddy conditions (Steinhardt et al., 2014). The Mg/Ca-derived shift
437 is hence larger than the shift inferred from $\delta^{18}O_{CC}$ (eddy: 107 m and non-eddy: 60 m). Mg/Ca-
438 derived calcification temperatures for *N. dutertrei* and *P. obliquiloculata* are hence cooler and
439 indicative of deeper calcification of the final chambers compared to that of the whole shell (based

on $\delta^{18}O_{cc}$). Calcification temperatures derived from Mg/Ca for *G. scitula* (Fig. 5), indicate an opposite trend, shifting between approximately 200 and 460 m (average 330 m) during eddy conditions to shallower depths between approximately 120 and 420 m (average 270 m) during non-eddy conditions (Steinhardt et al., 2014). Although the $\delta^{18}O_{cc}$ suggests calcification somewhat deeper than the Mg/Ca data, both Mg/Ca and $\delta^{18}O$-derived calcification depth indicate a shoaling for this species during non-eddy conditions. Furthermore, the average $\delta^{18}O$-derived calcification temperature of 10.4±3.9°C is in good agreement with previously published results for this species (Fallet et al. 2011; Birch et al. 2013). We refrain from correcting for a vital effect, as this would lower $\delta^{18}O$-derived calcification temperature to values unrealistically lower than the Mg/Ca-derived calcification temperatures for the last chambers. The observed remaining offset between single-specimen $\delta^{18}O$ and single chamber Mg/Ca in *G. scitula* suggest that either 1) there is a vital effect resulting in more enriched (i.e. positive) $\delta^{18}O$ values than when this species would precipitate its shell in isotopic equilibrium with seawater, 2) a more shallow calcification depth during formation of the final chamber, 3) that crust carbonate adds significantly to the total shell mass, or, 4) the Mg/Ca calibration for *G. hirsuta* (Anand et al., 2003) might be different from that of *G. scitula*. Following the vital effect correction of Williams and Kahn (1981), calcification temperature is 6.4°C±3.9°C, which is equivalent to an average calcification depth for *G. scitula* between 600 and deeper than 1100 m. This is in agreement with a suggested depth habitat within the upper 1000 m for this species (Schiebel et al., 1995; Ortiz et al., 1996; Itou et al., 2001). In our opinion the last two explanations are most likely, however, irrespective of the underlying mechanism it is clear that the majority of the test carbonate precipitated at a depth greater or comparable to that of the ontogenetic carbonate of the final chambers.

The range of uncertainties related to a species' average calcification depth results from the relatively large natural inter-specimen variability in Mg/Ca. Since we focus on relative differences within species between hydrographic conditions, the uncertainty in calcification temperature resulting from errors in the applied Mg/Ca-temperature calibration does not affect the absolute temperature differences between the eddy- and non-eddy conditions. Instead, uncertainties in the calculated difference in calcification depths between species will be caused by the inter-specimen variability in Mg/Ca.

5.3.1 Cumulative calcification model

We used a conceptual oxygen isotope mass balance model (Wilke, 2006; 2009), applying the temperature fractionation from inorganic calcite precipitation of Kim and O'Neil (1997) to our measured $\delta^{18}O_{CC}$. The model equation describing foraminiferal migration as a function of depth

used here is known as the cumulative form of the Weibull function (Weibull, 1939). It is a continuous probability function (Eq. 4), relating the shell mass 'M' to depth (z) using two constants (α and β) determining the shape of this relationship:

(4) $M(z) = 1 - \exp(-1*(z/\beta)^{\alpha})$

Since shell size of planktonic foraminifera is thought to increase with water depth (Hemleben and Bijma, 1994; Peeters and Brummer, 2002) shell mass must also increase with depth. The isotopic composition of a single shell thus represents the weighted sum of equilibrium calcite precipitated over a depth range of the productive zone (i.e. where primary calcite formation takes place).
Based on equation (5), the expected stable isotope composition of a specimen for a discrete water depth interval can be calculated as follows:

(5) $\delta^{18}O_{model} = \sum_{i}^{n} \frac{(M_i - M_{i-1}) + \delta^{18}O_{eq,i}}{M_i}$

Given the $\delta^{18}O_{eq}$ profile in the water column and the measured $\delta^{18}O_{cc}$ of the planktonic foraminifera it is possible to model the mass development (growth pattern) by using the determined Mg/Ca calcification depth of the last chambers, indicating the base of the calcite production zone. The Mg/Ca-based temperature of the F-1 chamber was used to delimit 95% of the calcite production. In equation (5), $\delta^{18}O_{eq,i}$ denotes the interval averaged $\delta^{18}O$ of equilibrium calcite for the specified depth interval. For convenience, shell mass at the sea surface was taken as zero and modelled $\delta^{18}O_{cc}$ was done by adapting the variables 'α' and 'β' in equation 5.
Increasing the value of 'α' results in a growth curve with a narrow calcification range. Higher values for 'β' result in a deepening of the growth curve, thereby determining the position of the base of the productive zone. In contrast to Wilke's (Wilke et al., 2006; 2009) approach, we have determined the calcification temperatures of the last three to four chambers, which were used to constrain the base of the calcification range and hence constrained values for 'β'.
In this model, it is assumed that shell growth always follows the same function, which is continuous and does not differ between species. Offsets between $\delta^{18}O_{CC}$ and $\delta^{18}O_{sw}$ from expected equilibrium ('the vital effect'), is assumed to be constant over the temperature range in which the species calcifies. We have adapted $\delta^{18}O_{sw}$ in meter steps as calculated from *in situ* salinity measurements, which where interpolated for the upper 2000 meters. We have used expected $\delta^{18}O_{eq}$ values of eddy and non-eddy condition to compare depth distributions for all four species of planktonic foraminifera.

Calcification depths inferred from the cumulative $\delta^{18}O$ model (Fig. 7) match previously published calcification depths and associated temperatures for each of the species relatively well (e.g. Cléroux et al., 2008; 2013; Wilke et al., 2009; Fallet et., 2010; 2011; Birch et al., 2013). In three species, measured $\delta^{18}O_{CC}$ values reflect shallower calcification depths than do single-chamber Mg/Ca-based calcification depths, which is consistent with the general model of migration to greater depth during growth. In case of the deep dwelling *G. scitula,* however, $\delta^{18}O$-based calcification depth is below that of the final chambers as derived from Mg/Ca-temperatures. Without applying a temperature correction for $\delta^{18}O$-based calcification temperatures of *G. scitula*, calcification depth based on $\delta^{18}O_{CC}$ can deviate up to 300 m from the Mg/Ca based depths. This would suggest that the majority of the previously formed calcite was precipitated deeper in the water column. The model shows that species modulate their calcification pattern depending on the hydrographical conditions they live in (e.g. eddy, non-eddy condition). For *G. ruber*, our results show that this species seems to be an exclusive surface dweller and hence an application of the cumulative calcification model only confirms that the majority of the calcite is formed at the sea surface.

For the thermocline dwelling species *N. dutertrei* we find that this species calcifies most of its calcite in a narrow depth range. Our model indicates that calcification during eddy conditions is more intense in the deeper part of the thermocline (α= 8.8; β= 85), whereas calcification during non-eddy condition is more equally distributed over the entire thermocline (α= 1.9; β= 47). It is noteworthy that *N. dutertrei* appears to intensify its calcification efforts during eddy conditions deeper in the thermocline, matching well with the deepening of the isopycnals and hence a narrower range of optimal calcification conditions (Steinhardt et al., 2014). This calcification response is also reflected in more enriched $\delta^{13}C$ values during eddy conditions. For *P. obliquiloculata* modelled α and β values are relatively high, particularly during eddy conditions (α= 5.25; β= 133, compared to α= 3.1; β= 63 for non-eddy conditions). This indicates that most of the calcification in *P. obliquiloculata* takes place at a water depth around 125 m during eddy conditions, and around 50 m during non-eddy conditions. The range at which *G. scitula* calcifies is well below the seasonal thermocline, reflected by high values for α and β (Fig. 7) and does not vary considerably during eddy and non-eddy conditions.

In general, we conclude that temperature changes within the thermocline induced by eddies affect non-symbiotic species mostly. Also, changes in cumulative calcite addition with depth seem to be species-specific. We modified the model by including Mg/Ca-based temperatures (following the species specific equations of Anand et al., 2003) of the F-1 chamber to constrain the 95% calcification level. This allows to predict expected $\delta^{18}O_{eq}$ for different species and shell sizes

(Spero et al., 1997; Bijma et al., 1999; Itou et al., 2001; Peeters et al., 2002). The extended version of the model does not distinguish between calcite deposited during chamber formation (primary calcite) and calcite added as a result of wall thickening due to gametogenic calcite or the precipitation of crust (secondary calcite, Bé, 1980; Duplessy et al., 1981; Lohmann, 1995, Jonkers et al., 2012). Secondary calcification might play an important role for deeper dwelling species such as *G. scitula*, which could explain the offset (about 1‰) between $\delta^{18}O_{model}$ and $\delta^{18}O_{CC}$. This suggests that relatively more calcite is formed deeper in the water column, or secondary calcite is precipitated with a fundamentally different calcification mechanism.

5.3.2 Carbon isotopes – testing the calcification model

The $\delta^{13}C$ values found in planktonic foraminifera is primarily a function of the carbon isotope composition of the dissolved inorganic carbon (DIC) in seawater (e.g. Urey, 1947; Epstein et al., 1953; McCorkle et al., 1990), which changes with water depth (e.g. Fairbanks et al., 1980, Curry and Crowley, 1987). Therefore, we can use the cumulative mass balance model output of the mass added per meter to calculated $\delta^{13}C_{expect}$ as the weighted sum of the $\delta^{13}C_{DIC}$ (Wilke et al., 2006). Depth-resolved carbon isotope composition ($\delta^{13}C_{DIC}$), available from locations closest to our study site (locations between 37-43 °E and 24.7 °S, World Ocean Database 2009) were used to calculate the expected $\delta^{13}C$ of each species of foraminifera ($\delta^{13}C_{expect}$). Since there is no relation between size and stable carbon isotopes in our specimens, the employed size fractions contained only mature (adult) specimens (Brummer et al., 1986, 1987). Comparing water column $\delta^{13}C_{DIC}$ data (Supplement, Fig. A1) from several stations near the MC reveals that absolute values and depth range over which values decrease is similar at the different sites. To verify the depth related calcification model we compare measured $\delta^{13}C_{CC}$ with model-based $\delta^{13}C_{expect}$ values (Fig. 8).

Carbon isotope values become more negative from surface dwelling *G. ruber* towards deeper dwelling *P. obliquiloculata* near the upper thermocline. Conversely, the $\delta^{13}C$ of *Globorotalia scitula* increases with depth. Low temperatures and reduced food availability have been suggested to result in relatively low metabolic rates in deep dwelling species, so that their $\delta^{13}C$ likely approaches $\delta^{13}C_{DIC}$ values (Birch et al., 2013). This suggests the involvement of biological controls on the $\delta^{13}C$ of the different genera (*Globigerinoides, Neogloboquadrina, Pulleniatina and Globorotalia*). All $\delta^{13}C_{expect}$ are higher than the measured $\delta^{13}C_{CC}$.

Our cumulative mass balance shows that the majority of the carbonate of *G. ruber* is formed in surface waters (Fig. 7). Equal $\delta^{13}C_{expect}$ values for eddy and non-eddy conditions are the result of similarly enriched $\delta^{13}C_{DIC}$ in the mixed layer. The measured differences in $\delta^{13}C_{CC}$ (Fig. 8) are likely

a consequence of the deepening thermocline during passage of an eddy, carrying nutrient-depleted waters (Kolasinski et al., 2013). Anticyclonic eddies are characterized by accumulation of warm, nutrient-poor and chlorophyll-depleted water in the center, which implies that also $\delta^{13}C_{DIC}$ is more isotopically enriched. Still, local nutrient enrichment potentially occurs at the outer edge as a result of high turbulence along the isopycnal slope (e.g. Falkowski et al., 1991; Lévy, 2003). The strong response of the Mg/Ca and $\delta^{18}O$ of *N. dutertrei* during eddy conditions (deeper calcification) is also reflected by more depleted δ^{13}Ccc values. Remineralization of organic matter at greater depth cause enrichment of $\delta^{13}C_{DIC}$, resulting in the incorporation of lighter carbon isotopes into the shell of *N. dutertrei* during eddy conditions. Based on samples from a sediment trap in Cape basin, Wilke et al. (2009) showed that the species *N. dutertrei* is an accurate recorder of the $\delta^{13}C_{DIC}$. This is in agreement with previous findings (Mulitza et al., 1999), showing that the carbon isotopic composition of *N. dutertrei* exhibits a constant and temperature-independent off-set from $\delta^{13}C_{DIC}$ of ~0.5‰ over a wide temperature range. This difference is in line with the offset in our dataset between $\delta^{13}C_{expect}$ and $\delta^{13}C_{CC}$ of *N. dutertrei* (0.6‰).

The $\delta^{13}C$ of the symbiont-barren *G. scitula* significantly deviates from those of the shallower dwelling species as a result of a decrease in $\delta^{13}C_{DIC}$ with water depth (see supplementary information, Fig. A1 and A2). The more depleted $\delta^{13}C_{CC}$ of *G. scitula* may also be a consequence of a lower metabolism of this species (Vergnaud-Grazzini, 1976; Kahn, 1977, 1979; Berger et al, 1978; Erez, 1978) compared to that of *G. ruber* and *N. dutertrei*. At high metabolic activity, more isotopically lighter carbon is incorporated and since lower temperatures usually reduce metabolic rates, species inhabiting deeper water depths may incorporate relatively heavier carbon isotopes. Minor changes in $\delta^{13}C_{cc}$ for *G. scitula* during eddy versus non-eddy conditions are in line with the minor response in calcification depth for this species. Similar to previous conclusions, this suggests that Mg/Ca inferred temperature differences between *N. dutertrei* and *G. scitula* are good indicators for eddies passing (Steinhardt et al., 2014). In addition, the $\delta^{13}C_{CC}$ differences between these species might very well help to reconstruct eddy frequency in this area. The depth integrated difference between $\delta^{13}C$ of *N. dutertrei* and *G. scitula* changes from 0.25 to 0.05 ‰.

Comparing $\delta^{13}C_{expect}$ and $\delta^{13}C_{CC}$ for *P. obliquiloculata* there is a discrepancy between eddy and non-eddy conditions (Fig. 8). Similar to *N. dutertrei*, this species is mostly associated with the thermocline (Anand et al., 2003; Cléroux et al., 2008; Sadekov et al., 2009). Our cumulative calcification model showed a slightly deeper calcification depth for *N. dutertrei* and a minor eddy response in calcification range (Fig. 7). However, $\delta^{13}C$ values indicate a significant difference between eddy and non-eddy conditions. Mulitza et al. (1999) showed that *P. obliquiloculata* does

not calcify in isotopic equilibrium with dissolved $\sum CO_2$, but the deviation from isotopic equilibrium is a linear function of temperature (Fig. 8). While the mean of the $\delta^{13}C$ cannot be used to infer the actual calcification depth, they argue that the spread and skewness of the individual $\delta^{13}C$ measurements should still be representative of the range of calcification depths and habitat preferences within the thermocline.

Also changes in the carbonate ion concentration with depth potentially play an important role in the observed differences between species and between eddy and non-eddy conditions (supplementary, Fig. A1 and A2). Since the carbonate ion profile is expected to change in accordance with thermocline deepening when an eddy passes we refrained from correcting for this. The observed offsets between species, however, suggest that carbonate ion does play a role there. The deeper living species show an increasing offset with respect to the 1:1 line (Fig. 8). The exception is *P. obliquiloculata* which responds to temperature rather than $\delta^{13}C_{DIC}$ carbonate ion changes (Mulitza et al., 1999).

Overall the here observed relations indicate that interpretation of the foraminifera vertical distribution in the upper water column can be unraveled by coupling various geochemical methods in order to retrieve calcification temperature at different stages in a foraminifera's life cycle. This in turn can be used to develop new proxies for the thermal and nutrient structure of the upper part of the water column.

6. Conclusion

Documenting changes in upper ocean stratification is essential for understanding past climatic conditions from sediment cores and is commonly estimated by determining the difference in $\delta^{18}O$ between thermocline and surface-dwelling planktonic foraminifera (Spero et al., 2003; Cléroux et al., 2007; Farmer et al., 2007; Lin and Hsieh, 2007; Steph et al., 2009). We conducted stable isotope measurements on four species of planktonic foraminifera (*G. ruber*, *N. dutertrei*, *P. obliquiloculata* and *G. scitula*) from selected sediment trap samples, representing eddy and non-eddy conditions in the MC.

Using single shell $\delta^{18}O_{CC}$ paired to single-chamber LA-ICP-MS Mg/Ca measurements we applied a cumulative mass balance model in order to compare growth patterns of the various planktonic species during eddy and non-eddy conditions. The results indicate that most of the species have somewhat different calcification patterns during eddy and non-eddy conditions. Only Mg/Ca values of *G. scitula* suggest higher calcification temperatures than inferred from $\delta^{18}O$. Furthermore, the results of the $\delta^{18}O$ cumulative mass balance model agree with previous findings that thermocline

dwelling *N. dutertrei* and deep dwelling *G. scitula* are suitable recorders of eddy induced hydrographic changes (Steinhardt et al., 2014). The combination of various proxies (e.g. Mg/Ca, $\delta^{18}O$ and $\delta^{13}C$) can thus provide a useful set of geochemical proxies to reconstruct the thermal and nutrient structure of the upper part of the water column.

All species analyzed have unique offsets from ambient seawater $\delta^{13}C$. However, comparison of species specific isotopic trajectories with water column $\delta^{13}C$ reveals that ambient $\delta^{13}C_{DIC}$ may be recorded by the species used in this study. The $\delta^{13}C$ of *N. dutertrei* and *G. scitula* show eddy related changes in their offsets and can potentially aid to unravel eddy related changes in the nutrient structure.

The Supplement related to this article is available online at doi:10.5194/bgd-11-17255-2014-supplement.

Acknowledgements. We acknowledge funding from the European Commission 7th Framework Marie Curie People program FP7/2007–2013 through funding of the Initial Training Network "GATEWAYS" (http://www.gateways-itn.eu) under the grant number 238512. Furthermore we acknowledge funding from the LOCO and INATEX programs by the Netherlands Organisation for Scientific Research. Analyses and visualizations of satellite SST used in this paper were produced with the Giovanni online data system, developed and maintained by the NASA GES DISC. We thank the chief scientist Herman Ridderinkhof and the crew of the RRV Charles Darwin, RRV Discovery, FS Meteor, RV Pelagia and R/V Algoa. Great thanks to Helen de Waard and Michiel Kienhuis for providing technical support with the trace element analysis at Utrecht University and Suzanne Verdegaal for supporting the measurements at the Vrije Universiteit Amsterdam.

References:

Anand, P., Elderfield, H. and Conte, M.: Calibration of Mg/Ca thermometry in planktonic foraminifera from a sediment trap time series, Paleoceanography, 18, 28–31, 2003.

Anand, P., Kroon, D., Singh, A., Ganeshram, R., Ganssen, G., and Elderfield, H.: Coupled sea surface temperature–seawater *δ¹⁸O* reconstructions in the Arabian Sea at the millennial scale for the last 35 ka, Paleoceanography, 23, PA4207, doi: 10.1029/2007PA001564, 2008.

Backeberg, B. and Reason, C.: A connection between the South Equatorial Current north of Madagascar and Mozambique Channel Eddies, Geophys. Res. Lett., 37, L04604, doi: 10.1029/2009GL041950, 2010.

Barker, S., Greaves, M. and Elderfield, H.: A study of cleaning procedures used for foraminiferal Mg/Ca paleothermometry, Geochem. Geophys. Geosystems, 4, 8407, 2003.

Bé, A. W.: Planktonic foraminifera, Antarct. Map Folio Ser. Am. Geogr. Soc., 9–12, 1969.

Bé, A. W. H.: An ecological, zoogeographic and taxonomic review of recent planktonic foraminifera, Ocean. Micropalaeontology, 1, 305-316, 1977.

Bé, A. W., Hemleben, C., Anderson, O. R. and Spindler, M.: Chamber formation in planktonic foraminifera, Micropaleontology, 25, 294–307, 1979.

Bé, A. W. H.: Gametogenic calcification in a spinose planktonic foraminifer, *Globigerinoides sacculifer* (Brady), Mar. Micropaleontol., 5, 283–310, doi:10.1016/0377-8398(80)90014-6, 1980.

Bé, A. W. and Spero, H. J.: Shell regeneration and biological recovery of planktonic foraminifera after physical injury induced in laboratory culture, Micropaleontology, 27, 305–316, 1981.

Bemis, B. E., Spero, H. J., Bijma, J. and Lea, D. W.: Reevaluation of the oxygen isotopic composition of planktonic foraminifera: Experimental results and revised paleotemperature equations, Paleoceanography, 13(2), 150–160, doi:10.1029/98PA00070, 1998.

Berger, W., Killingley, J. and Vincent, E.: Sable isotopes in deep-sea carbonates-box core erdc-92, west equatorial pacific, Oceanol. Acta, 1, 203–216, 1978.

Bijma, J., Spero, H. and Lea, D.: Reassessing foraminiferal stable isotope geochemistry: Impact of the oceanic carbonate system (experimental results), in Use of proxies in paleoceanography, pp. 489–512, Springer, Berlin Heidelberg, 1999.

Birch, H., Coxall, H. K., Pearson, P. N., Kroon, D. and O'Regan, M.: Planktonic foraminifera stable isotopes and water column structure: Disentangling ecological signals, Mar. Micropaleontol., 10, 127-145, 2013.

Brady, H.: Foraminifera in Tizard and Murray's Exploration of the Faroe Channel, vol. 11. In Proc. Roy. Soc, 1882.

Brady, H.: Foraminifera in Tizard and Murray's Exploration of the Faroe Channel, vol. 11. 1882.

Brummer, G.-J. A., Hemleben, C. and Spindler, M.: Planktonic foraminiferal ontogeny and new perspectives for micropalaeontology, Nature, 319(6048), 50–52, doi:10.1038/319050a0, 1986.

Brummer, G.-J. A., Hemleben, C. and Spindler, M.: Ontogeny of extant spinose planktonic foraminifera (Globigerinidae): A concept exemplified by *Globigerinoides sacculifer* (Brady) and *G. ruber* (d'Orbigny), Mar. Micropaleontol., 12, 357–381, doi:10.1016/0377-8398(87)90028-4, 1987.

Cléroux, C., Cortijo, E., Duplessy, J. and Zahn, R.: Deep-dwelling foraminifera as thermocline temperature recorders, Geochem. Geophys. Geosystems, 8, 2007.

Cléroux, C., Cortijo, E., Anand, P., Labeyrie, L., Bassinot, F., Caillon, N. and Duplessy, J.-C.: Mg/Ca and Sr/Ca ratios in planktonic foraminifera: Proxies for upper water column temperature reconstruction, Paleoceanography, 23, PA3214, doi: 10.1029/2007pa001505, 2008.

Cléroux, C., deMenocal, P., Arbuszewski, J. and Linsley, B.: Reconstructing the upper water column thermal structure in the Atlantic Ocean, Paleoceanography, 28(3), 503–516, doi: 10.1002/palo.20050, 2013.

Curry, W. B. and Crowley, T. J.: The $\delta^{13}C$ of equatorial Atlantic surface waters: Implications for ice age pCO_2 levels, Paleoceanography, 2, 489–517, 1987.

Curry, W. B., Thunell, R. C. and Honjo, S.: Seasonal changes in the isotopic composition of planktonic foraminifera collected in Panama Basin sediment traps, Earth Planet. Sci. Lett., 64, 33–43, doi: 10.1016/0012-821X(83)90050-X, 1983.

716 Damassa, T. D., Cole, J. E., Barnett, H. R., Ault, T. R. and McClanahan, T. R.: Enhanced multidecadal
717 climate variability in the seventeenth century from coral isotope records in the western Indian Ocean,
718 Paleoceanography, 21, PA2016, doi: 10.1029/2005PA001217, 2006.
719 Deuser, W. G.: Variability of hydrography and particle flux: Transient and long-term relationships, Mitt. Geol.-
720 Palaeont. Inst. Univ. Hambg., 62, 179–193, 1987.
721 Deuser, W. G. and Ross, E. H.: Seasonally abundant planktonic foraminifera of the Sargasso Sea;
722 succession, deep-water fluxes, isotopic compositions, and paleoceanographic implications, J. Foraminifer.
723 Res., 19, 268–293, doi: 10.2113/gsjfr.19.4.268, 1989.
724 Deuser, W., Ross, E., Hemleben, C. and Spindler, M.: Seasonal changes in species composition, numbers,
725 mass, size, and isotopic composition of planktonic foraminifera settling into the deep Sargasso Sea,
726 Palaeogeogr. Palaeoclimatol. Palaeoecol., 33, 103–127, 1981.
727 Duplessy, J. C., Bé, A. W. H. and Blanc, P. L.: Oxygen and carbon isotopic composition and biogeographic
728 distribution of planktonic foraminifera in the Indian Ocean, Palaeogeogr. Palaeoclimatol. Palaeoecol., 33,
729 9–46, doi: 10.1016/0031-0182(81)90031-6, 1981.
730 Durgadoo, J.V., Loveday, B.R., Reason, C.J., Penven, P., Biastoch, A.: Agulhas leakage predominantly
731 responds to the Southern Hemisphere Westerlies. J. Phys. Oceanogr. 43, 2113–2131.
732 http://dx.DOI.org/10.1175/JPO-D-13-047.1, 2013
733 Eggins, S., De Deckker, P. and Marshall, J.: Mg/Ca variation in planktonic foraminifera tests: Implications
734 for reconstructing palaeo-seawater temperature and habitat migration, Earth Planet. Sci. Lett., 212, 291–
735 306, 2003.
736 Eguchi, N. O., Ujiié, H., Kawahata, H. and Taira, A.: Seasonal variations in planktonic foraminifera at three
737 sediment traps in the subarctic, transition and subtropical zones of the central North Pacific Ocean, Mar.
738 Micropaleontol., 48, 149–163, 2003.
739 Elderfield, H., Bertram, C. J. and Erez, J.: A biomineralization model for the incorporation of trace elements
740 into foraminiferal calcium carbonate, Earth Planet. Sci. Lett., 142, 409–423, doi: 10.1016/0012-
741 821X(96)00105-7, 1996.
742 Elderfield, H. and Ganssen, G.: Past temperature and ^{18}O of surface ocean waters inferred from
743 foraminiferal Mg/Ca ratios, Nature, 405, 442–445, 2000.
744 Emiliani, C.: Depth habitats of some species of pelagic Foraminifera as indicated by oxygen isotope ratios,
745 Am. J. Sci., 252, 149–158, doi: 10.2475/ajs.252.3.149, 1954.
746 Epstein, S. and Mayeda, T.: Variation of O^{18} content of waters from natural sources, Geochim. Cosmochim.
747 Acta, 4, 213–224, 1953.
748 Erez, J.: Vital effect on stable-isotope composition seen in foraminifera and coral skeletons, Nature 273,
749 199-202, doi:10.1038/273199a0, 1978.
750 Erez, J.: The source of ions for biomineralization in foraminifera and their implications for paleoceanographic
751 proxies, Rev. Mineral. Geochem., 54, 115–149, 2003.

752 Erez, J. and Honjo, S.: Comparison of isotopic composition of planktonic foraminifera in plankton tows,
753 sediment traps and sediments, Palaeogeogr. Palaeoclimatol. Palaeoecol., 33, 129–156, doi:10.1016/0031-
754 0182(81)90035-3, 1981.
755 Fairbanks, R. G., Wiebe, P. H. and Bé, A. W.: Vertical distribution and isotopic composition of living
756 planktonic foraminifera in the western North Atlantic, Science, 207, 61–63, 1980.
757 Fairbanks, R. G., Sverdlove, M., Free, R., Wiebe, P. H. and Bé, A. W.: Vertical distribution and isotopic
758 fractionation of living planktonic foraminifera from the Panama Basin, Nature, 298, 841–844, 1982.
759 Falkowski, P. G., Ziemann, D., Kolber, Z. and Bienfang, P. K.: Role of eddy pumping in enhancing primary
760 production in the ocean, Nature 352, 55-58, doi:10.1038/352055a0, 1991.
761 Fallet, U., Boer, W., van Assen, C., Greaves, M. and Brummer, G.-J. A.: A novel application of wet oxidation
762 to retrieve carbonates from large organic-rich samples for ocean-climate research, Geochem Geophys
763 Geosyst, 10, Q08004, doi: 10.1029/2009gc002573, 2009.
764 Fallet, U., Brummer, G.-J., Zinke, J., Vogels, S. and Ridderinkhof, H.: Contrasting seasonal fluxes of
765 planktonic foraminifera and impacts on paleothermometry in the Mozambique Channel upstream of the
766 Agulhas Current, Paleoceanography, 25, PA4223, doi: 10.1029/2010pa001942, 2010.
767 Fallet, U., Ullgren, J. E., Castañeda, I. S., van Aken, H. M., Schouten, S., Ridderinkhof, H. and Brummer,
768 G.-J. A.: Contrasting variability in foraminiferal and organic paleotemperature proxies in sedimenting
769 particles of the Mozambique Channel (SW Indian Ocean), Geochim. Cosmochim. Acta, 75, 5834–5848,
770 2011.
771 Fallet, U., Castañeda, I. S., Henry-Edwards, A., Richter, T. O., Boer, W., Schouten, S. and Brummer, G.-J.:
772 Sedimentation and burial of organic and inorganic temperature proxies in the Mozambique Channel, SW
773 Indian Ocean, Deep Sea Res. Part Oceanogr. Res. Pap., 59, 37–53, 2012.
774 Farmer, E. C., Kaplan, A., de Menocal, P. B. and Lynch-Stieglitz, J.: Corroborating ecological depth
775 preferences of planktonic foraminifera in the tropical Atlantic with the stable oxygen isotope ratios of core
776 top specimens, Paleoceanography, 22(3), doi:DOI: 10.1029/2006PA001361, 2007.
777 Faul, K. L., Ravelo, A. C. and Delaney, M. L.: Reconstructions of Upwelling, Productivity, and Photic Zone
778 Depth in the Eastern Equatorial Pacific Ocean Using Planktonic Foraminiferal Stable Isotopes and
779 Abundances, J. Foraminifer. Res., 30, 110–125, doi: 10.2113/0300110, 2000.
780 Field, D. B.: Variability in vertical distributions of planktonic foraminifera in the California Current:
781 Relationships to Vertical Ocean structure, Paleoceanography, 19, PA2014, doi:10.1029/2003PA000970,
782 2004.
783 Friedrich, O., Schiebel, R., Wilson, P. A., Weldeab, S., Beer, C. J., Cooper, M. J. and Fiebig, J.: Influence
784 of test size, water depth, and ecology on Mg/Ca, Sr/Ca, $\delta^{18}O$ and $\delta^{13}C$ in nine modern species of planktic
785 foraminifers, Earth Planet. Sci. Lett., 319, 133–145, doi: 10.1016/j.epsl.2011.12.002, 2012.
786 Ganssen, G. and Sarnthein, M.: Stable-Isotope Composition of Foraminifers: The Surface and Bottom Water
787 Record of Coastal Upwelling, in Coastal Upwelling Its Sediment Record, edited by E. Suess and J. Thiede,
788 pp. 99–121, Springer US. [online] Available from: http://link.springer.com/chapter/10.1007/978-1-4615-
789 6651-9_6 (Accessed 5 December 2013), 1983.

Grossman, E. L.: Stable isotopes in modern benthic foraminifera; a study of vital effect, J. Foraminifer. Res., 17, 48–61, 1987.

Gründlingh, M. L.: Tracking eddies in the southeast Atlantic and southwest Indian oceans with TOPEX/POSEIDON, J. Geophys. Res., 100, 24977–24,986, 1995.

Hastenrath, S., Nicklis, A. and Greischar, L.: Atmospheric-hydrospheric mechanisms of climate anomalies in the western equatorial Indian Ocean, J. Geophys. Res. Oceans, 98, 20219–20235, doi: 10.1029/93JC02330, 1993.

Hathorne, E. C., James, R. H. and Lampitt, R. S.: Environmental versus biomineralization controls on the intratest variation in the trace element composition of the planktonic foraminifera *G. inflata* and *G. scitula*, Paleoceanography, 24, PA4204, doi: 10.1029/2009pa001742, 2009.

Hemleben, C. and Bijma, J.: Foraminiferal population dynamics and stable carbon isotopes, in Carbon Cycling in the Glacial Ocean: Constraints on the Ocean's Role in Global Change, Springer, Berlin Heidelberg, 145–166, 1994.

Hemleben, C., Spindler, M. and Anderson, O.: Modern planktonic foraminifera, Springer, Berlin, 363 pp., 1989.

Huang, K., You, C., Lin, H. and Shieh, Y.: In situ calibration of Mg/Ca ratio in planktonic foraminiferal shell using time series sediment trap: A case study of intense dissolution artifact in the South China Sea, Geochem. Geophys. Geosystems, 9, Q04016, doi:10.1029/207GC001660, 2008.

Hut, G.: Stable Isotope Reference Samples for Geochemical and Hydrological Investigations. Rep. to Dir. Gen., International Atomic Energy Agency, Vienna, 42 pp., 1987.

Itou, M., Ono, T., Oba, T. and Noriki, S.: Isotopic composition and morphology of living *Globorotalia scitula*: a new proxy of sub-intermediate ocean carbonate chemistry?, Mar. Micropaleontol., 42, 189–210, 2001.

Jonkers, L., de Nooijer, L., Reichart, G., Zahn, R. and Brummer, G.: Encrustation and trace element composition of *Neogloboquadrina dutertrei* assessed from single chamber analyses, implications for paleotemperature estimates, Biogeosciences, 9, 4851–4860, doi:10.5194/bg-9-4851-2012, 2012.

Kahn, M. I.: Non-equilibrium oxygen and carbon isotopic fractionation in tests of living planktic foraminifera from the eastern equatorial Atlantic Ocean, Ph.D. thesis, University of South California, Los Angeles,224 p., 1977.

Kahn, M.: Non-equilibrium oxygen and carbon isotopic fractionation in tests of living planktonic-foraminifera, Oceanol. Acta, 2, 195–208, 1979.

Kahn, M. I. and Williams, D. F.: Oxygen and carbon isotopic composition of living planktonic foraminifera from the northeast Pacific Ocean, Palaeogeogr. Palaeoclimatol. Palaeoecol., 33, 47–69, 1981.

Kiefer, T., McCave, I. N. and Elderfield, H.: Antarctic control on tropical Indian Ocean sea surface temperature and hydrography, Geophys. Res. Lett., 33, L24612, doi:10.1029/2006GL027097, 2006.

Kim, S.-T. and O'Neil, J. R.: Equilibrium and nonequilibrium oxygen isotope effects in synthetic carbonates, Geochim. Cosmochim. Acta, 61, 3461–3475, doi: 10.1016/S0016-7037(97)00169-5, 1997.

826 Kolasinski, J., Kaehler, S. and Jaquemet, S.: Distribution and sources of particulate organic matter in a
827 mesoscale eddy dipole in the Mozambique Channel (south-western Indian Ocean): Insight from C and N
828 stable isotopes, J. Mar. Syst., 96-97, 122-131, doi:10.1016/j.jmarsys.2012.02.015, 2012.
829 Kroon, D. and Darling, K.: Size and upwelling control of the stable isotope composition *of Neogloboquadrina*
830 *dutertrei* (d'Orbigny), *Globigerinoides ruber* (d'Orbigny) and *Globigerina bulloides* d'Orbigny; examples from
831 the Panama Basin and Arabian Sea, J. Foraminifer. Res., 25, 39–52, 1995.
832 Kunioka, D., Shirai, K., Takahata, N., Sano, Y., Toyofuku, T. and Ujiie, Y.: Microdistribution of Mg/Ca, Sr/Ca,
833 and Ba/Ca ratios in *Pulleniatina obliquiloculata* test by using a NanoSIMS: Implication for the vital effect
834 mechanism, Geochem. Geophys. Geosystems, 7, Q12P20, doi:10.1029/2006GC001280, 2006.
835 Kuroyanagi, A. and Kawahata, H.: Vertical distribution of living planktonic foraminifera in the seas around
836 Japan, Mar. Micropaleontol., 53, 173–196, doi: 10.1016/j.marmicro.2004.06.001, 2004.
837 Lévy, M.: Mesoscale variability of phytoplankton and of new production: Impact of the large-scale nutrient
838 distribution, J. Geophys. Res. Oceans 1978–2012, 108, 3358, doi:10.1029/2002JC001577, 2003.
839 Lin, H.-L. and Hsieh, H.-Y.: Seasonal variations of modern planktonic foraminifera in the South China Sea,
840 Deep Sea Res. Part II Top. Stud. Oceanogr., 54, 1634–1644, 2007.
841 Lohmann, G. P.: A model for variation in the chemistry of planktonic foraminifera due to secondary
842 calcification and selective dissolution, Paleoceanography, 10(3), 445–457, doi:10.1029/95PA00059, 1995.
843 Lončarić, N., van Iperen, J., Kroon, D. and Brummer, G.-J. A.: Seasonal export and sediment preservation
844 of diatomaceous, foraminiferal and organic matter mass fluxes in a trophic gradient across the SE Atlantic,
845 Prog. Oceanogr., 73, 27–59, 2007.
846 Lončarić, N., Peeters, F. J. C., Kroon, D. and Brummer, G. J. A.: Oxygen isotope ecology of recent planktic
847 foraminifera at the central Walvis Ridge (SE Atlantic), Paleoceanography, 21, 3009, 2006.
848 McClanahan, T. R.: Seasonality in East Africa's coastal waters., Mar. Ecol. Prog. Ser. Oldendorf, 44, 191–
849 199, 1988.
850 McCorkle, D. C., Keigwin, L. D., Corliss, B. H. and Emerson, S. R.: The influence of microhabitats on the
851 carbon isotopic composition of deep-sea benthic foraminifera, Paleoceanography, 5, 161–185, 1990.
852 Mohtadi, M., Hebbeln, D., Nuñez Ricardo, S. and Lange, C. B.: El Niño–like pattern in the Pacific during
853 marine isotope stages (MIS) 13 and 11?, Paleoceanography, 21, PA1015, doi:10.1029/2005PA001190,
854 2006.
855 Mulitza, S., Dürkoop, A., Hale, W., Wefer, G. and Niebler, H. S.: Planktonic foraminifera as recorders of past
856 surface-water stratification, Geology, 25, 335–338, doi: 10.1130/0091-7613, 1997.
857 Mulitza, S., Arz, H., Kemle-von Mücke, S., Moos, C., Niebler, H.-S., Pätzold, J. and Segl, M.: The South
858 Atlantic carbon isotope record of planktic foraminifera, in Use of Proxies in Paleoceanography, pp. 427–
859 445, Springer., 1999.
860 New, A., Alderson, S., Smeed, D. and Stansfield, K.: On the circulation of water masses across the
861 Mascarene Plateau in the South Indian Ocean, Deep Sea Res. Part Oceanogr. Res. Pap., 54, 42–74, 2007.

Oppo, D. W. and Fairbanks, R. G.: Carbon isotope composition of tropical surface water during the past 22,000 years, Paleoceanography, 4, 333–351, 1989.

D' Orbigny, A.: Foraminifères, Hist. Phys. Polit. Nat. Lî Cuba Bertrand Paris, 1839.

Ortiz, J., Mix, A., Rugh, W., Watkins, J. and Collier, R.: Deep-dwelling planktonic foraminifera of the northeastern Pacific Ocean reveal environmental control of oxygen and carbon isotopic disequilibria, Geochim. Cosmochim. Acta, 60, 4509–4523, 1996.

Patrick, A. and Thunell, R. C.: Tropical Pacific sea surface temperatures and upper water column thermal structure during the last glacial maximum, Paleoceanography, 12, 649–657, 1997.

Parker, W. K., Jones, T. R., Bailey, J. and Pourtales, F.: On some foraminifera from the north Atlantic and Arctic Oceans, including Davis Straits and Baffin's Bay, Philos. Trans. R. Soc. Lond., 155, 325–441, 1865.

Peeters, F. J. C. and Brummer, G.-J. A.: The seasonal and vertical distribution of living planktic foraminifera in the NW Arabian Sea, Geol. Soc. Lond. Spec. Publ., 195, 463–497, doi: 10.1144/GSL.SP.2002.195.01.26, 2002

Peeters, F., Brummer, G. and Ganssen, G.: The effect of upwelling on the distribution and stable isotope composition of *Globigerina bulloides* and *Globigerinoides ruber* (planktic foraminifera) in modern surface waters of the NW Arabian Sea, Glob. Planet. Change, 34, 269–291, 2002.

Ravelo, A. and Fairbanks, R.: Oxygen isotopic composition of multiple species of planktonic foraminifera: Recorders of the modern photic zone temperature gradient, Paleoceanography, 7, 815–831, 1992.

Ravelo, A. and Fairbanks, R.: Carbon isotopic fractionation in multiple species of planktonic foraminifera from core-tops in the tropical Atlantic, J. Foraminiferal Res. 25, 53–74, doi:10.2113/gsjfr.25.1.53, 1995.

Ravelo, A., Fairbanks, R. and Philander, S.: Reconstructing tropical Atlantic hydrography using planktontic foraminifera and an ocean model, Paleoceanography, 5, 409–431, 1990.

Regenberg, M., Steph, S., Nürnberg, D., Tiedemann, R. and Garbe-Schönberg, D.: Calibrating Mg/Ca ratios of multiple planktonic foraminiferal species with δ18O-calcification temperatures: Paleothermometry for the upper water column, Earth Planet. Sci. Lett., 278(3–4), 324–336, doi:10.1016/j.epsl.2008.12.019, 2009.

Reichart, G.-J., Jorissen, F., Anschutz, P. and Mason, P. R.: Single foraminiferal test chemistry records the marine environment, Geology, 31(4), 355–358, 2003.

Russell, A. D. and Spero, H. J.: Field examination of the oceanic carbonate ion effect on stable isotopes in planktonic foraminifera, Paleoceanography, 15(1), 43–52, 2000.

Sadekov, A., Eggins, S. M., De Deckker, P., Ninnemann, U., Kuhnt, W. and Bassinot, F.: Surface and subsurface seawater temperature reconstruction using Mg/Ca microanalysis of planktonic foraminifera *Globigerinoides ruber*, *Globigerinoides sacculifer*, and *Pulleniatina obliquiloculata*, Paleoceanography, 24, PA3201, doi:10.1029/2008PA001664, 2009.

Schmidt, G.A., G. R. Bigg and E. J. Rohling. 1999. "Global Seawater Oxygen-18 Database - v1.21" http://data.giss.nasa.gov/o18data/ (last access: 2 November 2014), 1999.

Shackleton, N.: Attainment of isotopic equilibrium between ocean water and the benthonic foraminifera genus *Uvigerina*: isotopic changes in the ocean during the last glacial, Les methods quantitatives d'etude

des variations du climat au cours du Pleistocene, Gif-sur-Yvette, Colloque international du CNRS, 219, 203–210, 1974.

Spero, H. J. and Lea, D. W.: Intraspecific stable isotope variability in the planktic foraminifera *Globigerinoides sacculifer*: Results from laboratory experiments, Mar. Micropaleontol., 22, 221–234, 1993.

Spero, H. J., Lerche, I. and Williams, D. F.: Opening the carbon isotope "vital effect" black box, 2, Quantitative model for interpreting foraminiferal carbon isotope data, Paleoceanography, 6, 639–655, 1991.

Spero, H. J., Bijma, J., Lea, D. W. and Bemis, B. E.: Effect of seawater carbonate concentration on foraminiferal carbon and oxygen isotopes, Nature, 390, 497–500, doi: 10.1038/37333, 1997.

Spero, H. J., Mielke, K. M., Kalve, E. M., Lea, D. W. and Pak, D. K.: Multispecies approach to reconstructing eastern equatorial Pacific thermocline hydrography during the past 360 kyr, Paleoceanography, 18, 1022, doi: 10.1029/2002PA000814, 2003.

Steinhardt, J., Cléroux, C., Ullgren, J., de Nooijer, L., Durgadoo, J. V., Brummer, G.-J. and Reichart, G.-J.: Anti-cyclonic eddy imprint on calcite geochemistry of several planktonic foraminiferal species in the Mozambique Channel, Mar. Micropaleontol., 113, 20–33, doi: 10.1016/j.marmicro.2014.09.001, 2014.

Steinke, S., Chiu, H., Yu, P., Shen, C., Löwemark, L., Mii, H. and Chen, M.: Mg/Ca ratios of two *Globigerinoides ruber* (white) morphotypes: Implications for reconstructing past tropical/subtropical surface water conditions, Geochem. Geophys. Geosystems, 6, Q11005, 2005.

Steph, S., Regenberg, M., Tiedemann, R., Mulitza, S. and Nürnberg, D.: Stable isotopes of planktonic foraminifera from tropical Atlantic/Caribbean core-tops: Implications for reconstructing upper ocean stratification, Mar. Micropaleontol., 71, 1–19, doi: 10.1016/j.marmicro.2008.12.004, 2009.

Swallow, J., Fieux, M. and Schott, F.: The boundary currents east and north of Madagascar: 1. Geostrophic currents and transports, J. Geophys. Res. Oceans, 93, 4951–4962, 1988.

Tedesco, K., Thunell, R., Astor, Y. and Muller-Karger, F.: The oxygen isotope composition of planktonic foraminifera from the Cariaco Basin, Venezuela: Seasonal and interannual variations, Mar. Micropaleontol., 62, 180–193, doi:10.1016/j.marmicro.2006.08.002, 2007.

Tolderlund, D. S. and Bé, A. W.: Seasonal distribution of planktonic foraminifera in the western North Atlantic, Micropaleontology, 17, 297–329, 1971.

Ullgren, J., van Aken, H., Ridderinkhof, H. and de Ruijter, W.: The hydrography of the Mozambique Channel from six years of continuous temperature, salinity, and velocity observations, Deep-Sea Res., 69, 36–50, 2012.

Urey, H. C.: The thermodynamic properties of isotopic substances, J. Chem. Soc. (1926–1965), 562–581, doi:10.1039/JR9470000562, 1947.

Vergnaud Grazzini, C.: Non-equilibrium isotopic compositions of shells of planktonic foraminifera in the Mediterranean Sea, Palaeogeogr. Palaeoclimatol. Palaeoecol., 20, 263–276, 1976.

Vincent, E. and Berger, W.: Planktonic foraminifera and their use in paleoceanography, The sea, 7, 1025–1119, 1981.

Watkins, J. M., Mix, A. C. and Wilson, J.: Living planktic foraminifera: tracers of circulation and productivity regimes in the central equatorial Pacific, Deep Sea Res. Part II Top. Stud. Oceanogr., 43, 1257–1282, 1996.

Weibull, W.: A statistical theory of the strength of materials, Ingeniorsvetenskaps Akadeniens Handlingar NR. 151, 1939.

Wefer, G. and Berger, W. H.: Isotope paleontology: growth and composition of extant calcareous species, Mar. Geol., 100, 207–248, 1991.

Wilke, I., Bickert, T. and Peeters, F. J.: The influence of seawater carbonate ion concentration [CO_3^{2-}] on the stable carbon isotope composition of the planktic foraminifera species *Globorotalia inflata*, Mar. Micropaleontol., 58, 243–258, 2006.

Wilke, I., Meggers, H. and Bickert, T.: Depth habitats and seasonal distributions of recent planktic foraminifers in the Canary Islands region (29°N) based on oxygen isotopes, Deep Sea Res., 56, 89–106, doi: 10.1016/j.dsr.2008.08.001, 2009.

Wyrtki, K.: Physical oceanography of the Indian Ocean, in The biology of the Indian Ocean, Springer, Berlin Heidelberg, 18–36,1973.

Figures:

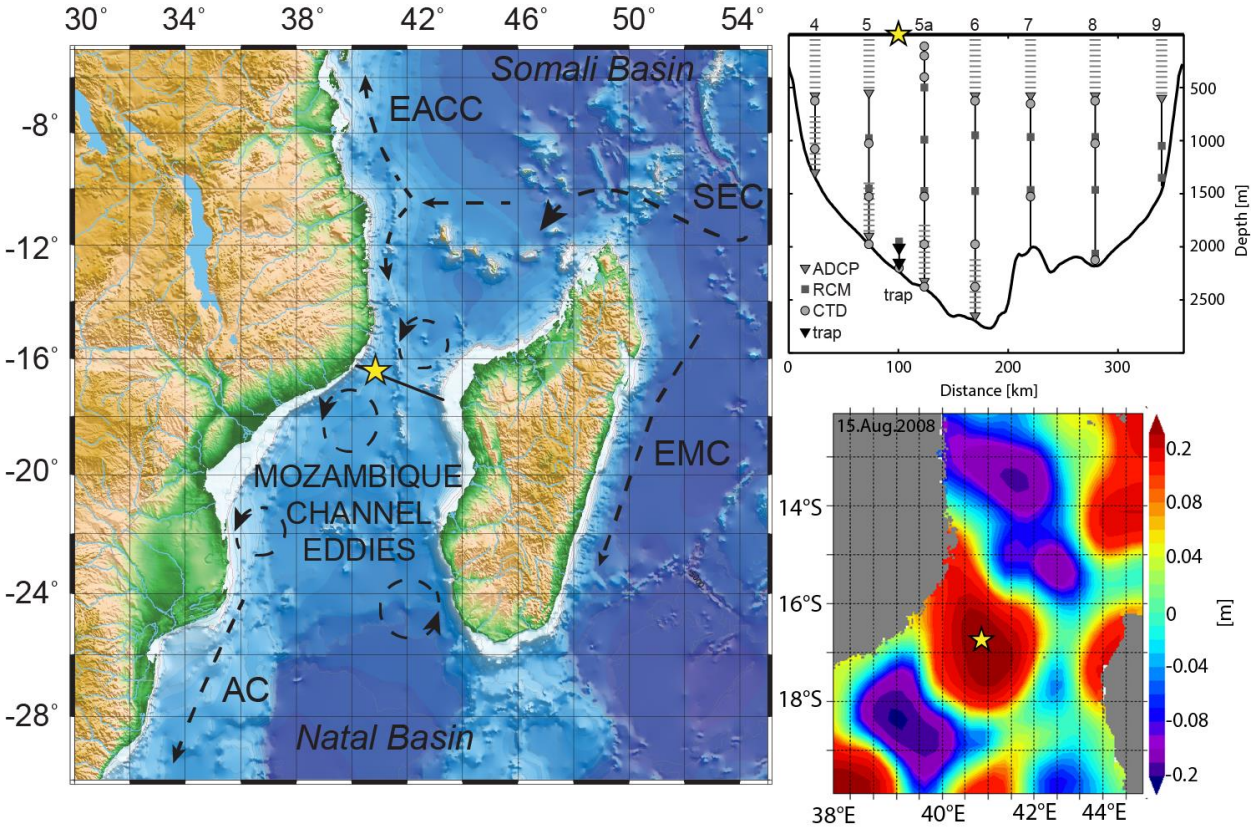

Fig. 1

species	Mg/Ca [mmol/mol]	Mg/Ca SD [mmol/mol]	Mg/Ca-based temperatures [°C]	$\delta^{18}O$ [‰]	$\delta^{18}O$ SD [‰]	$\delta^{18}O$-based temperatures [°C]	$\delta^{13}C$±SE [‰]	$\delta^{13}C$ SD [‰]
G. ruber	5.3±0.09	±1.2	28.1±2.8	-2.57±0.04	±0.35	29.4±1.3	0.51±0.03	±0.47
N. dutertrei	2.6±0.06	±1.0	22.5±3.7	-1.53±0.03	±0.48	24.3±2.0	0.53±0.04	±0.44
P. obliquiloculata	2.3±0.1	±0.6	21.6±3.1	-1.13±0.04	±0.24	22.3±1.1	0.04±0.04	±0.21
G. scitula	1.5±0.07	±0.4	14.4±3.4	1.47±0.14	±0.87	14.4±3.9*	0.27±0.04	±0.22

** vital effect corrected [Kahn an Williams, 1981]*

data from Steinhardt et al. 2014

954 *Tab. 1*

955

species	$\delta^{13}C$ [‰]		$\delta^{13}C$ SD [‰]		$\delta^{18}O$ [‰]		$\delta^{18}O$ SD [‰]	
	VU	BCN	VU	BCN	VU	BCN	VU	BCN
G. rub	-	0.51±0.03	-	±0.47	-	-2.57±0.04	-	0.35
N. dut	0.41±0.12	0.54±0.01	0.41	0.45	-1.37±0.09	-1.58±0.03	0.59	0.46
P. obli	-0.07±0.13	0.05±0.01	0.29	0.20	-1.46±0.09	-1.10±0.02	0.37	0.21
G. scit	0.13±0.14	0.3±0.02	0.24	0.21	1.55±0.11	1.45±0.04	0.69	0.92

956 Tab. 2

957

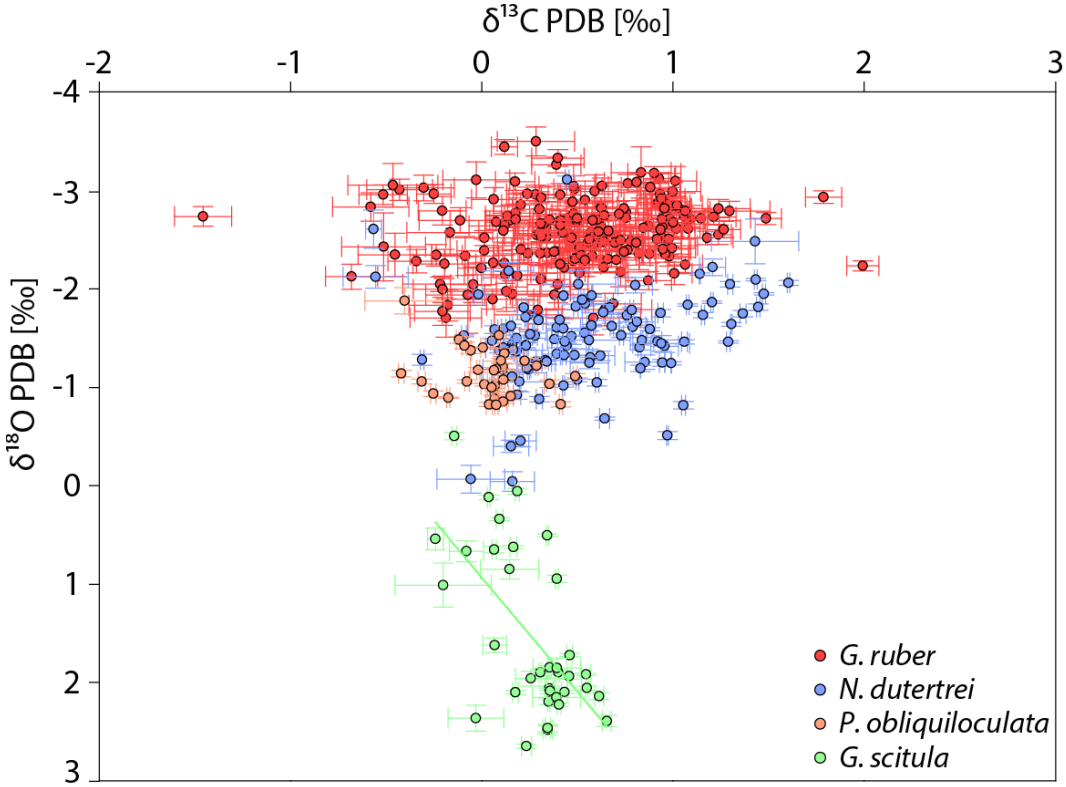
δ13C PDB [‰]
-2
-1
0
1
2
3
-4
-3
-2
-1
0
1
2
3
δ18O PDB [‰]
G. ruber
N. dutertrei
P. obliquiloculata
G. scitula

958

959 *Fig. 2*

Species	$\delta^{18}O \pm SE$ [‰]		$\delta^{18}O$ SD [‰]		T [°C], (Kim&O'Neil, 1997)		$\delta^{13}C \pm SE$ [‰]		$\delta^{13}C$ SD [‰]	
	Eddy	Non-Eddy	Eddy	Non-Eddy	Eddy	Non-Eddy	Eddy	Non-Eddy	Eddy	Non-Eddy
G. ruber	-2.56±0.03	-2.57±0.04	0.31	0.39	29.8	29.2	0.59±0.04	0.39±0.06	0.40	0.53
N. dutertrei	-1.53±0.08	-1.53±00.5	0.58	0.39	24.6	24.0	0.39±0.06	0.64±0.04	0.44	0.41
P. obliquiloculata	-1.25±0.06	-1.09±0.05	0.19	0.25	23.3	21.9	0.18±0.06	-0.02±0.04	0.18	0.19
G. scitula	1.99±0.1	1.18±0.2	0.48	0.92	8.2	11.5	0.31±0.05	0.25±0.06	0.18	0.26

960 *Tab. 3*

961

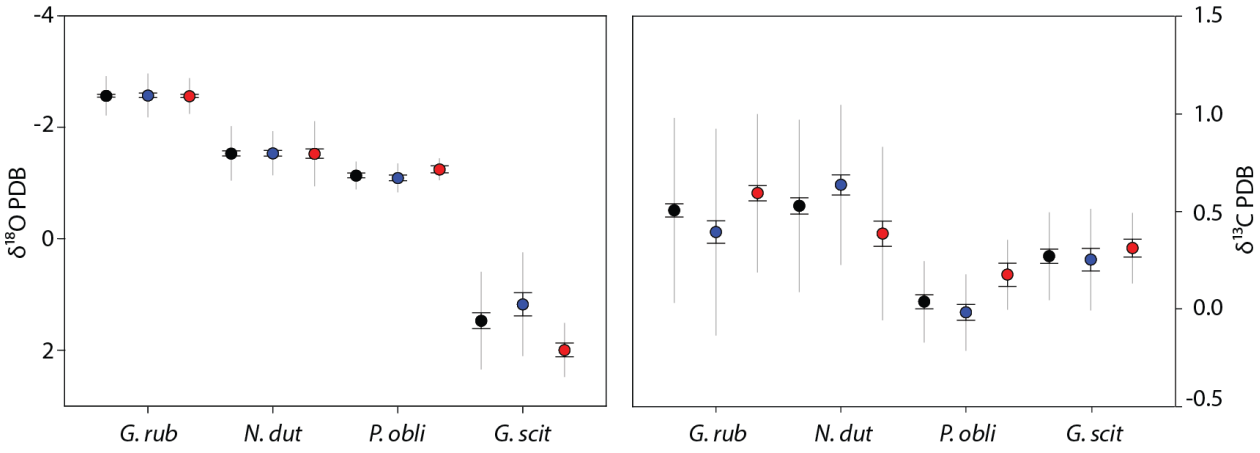

962

963

964 *Figure 3*

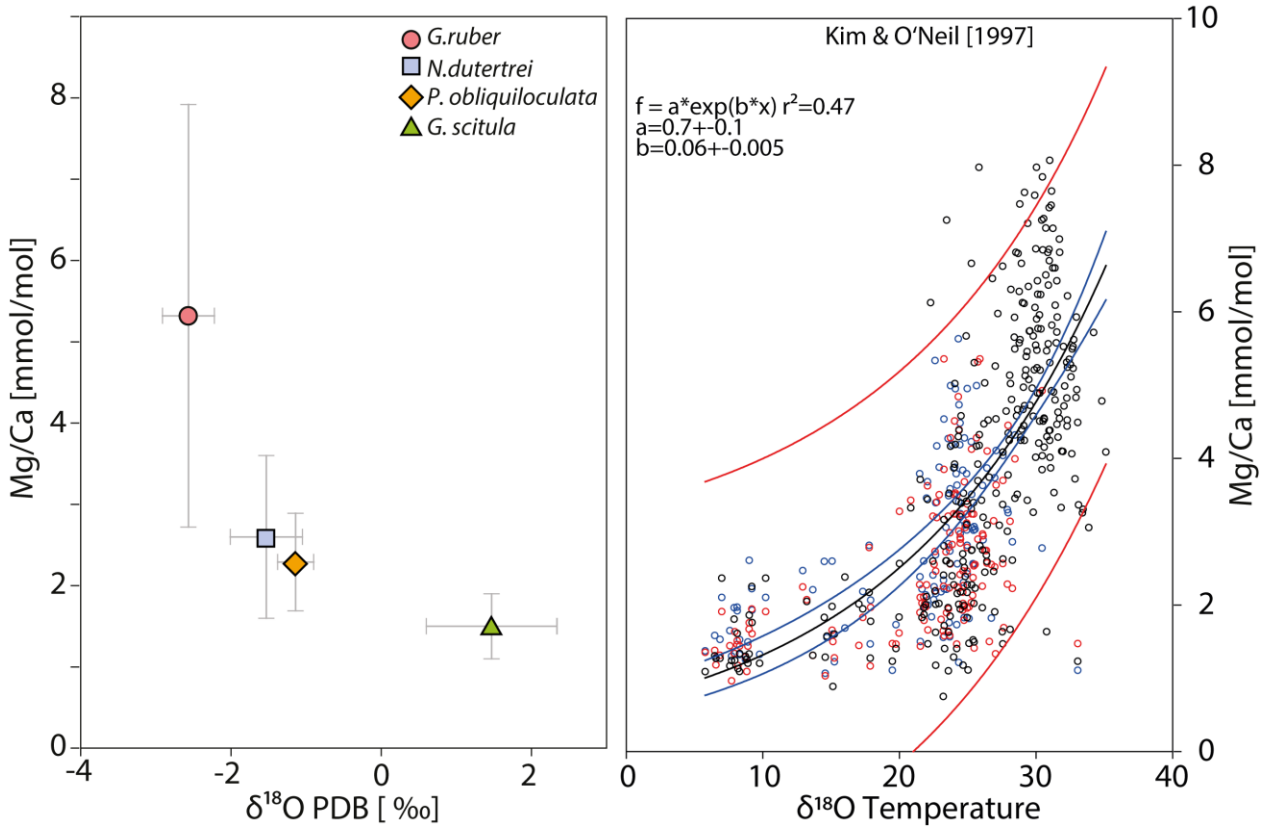

965

966 *Figure 4*

967

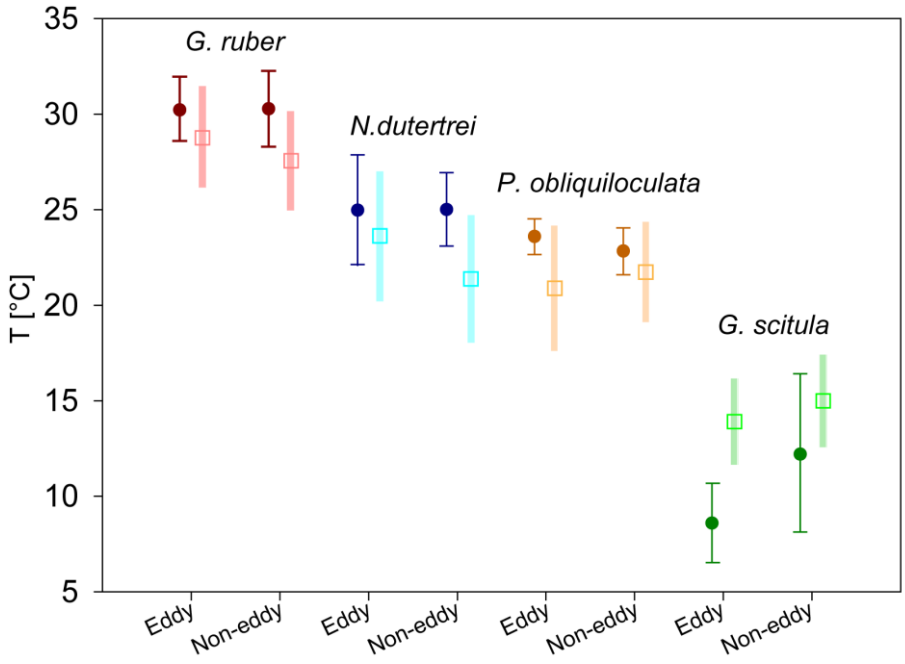

968

969 *Figure 5*

970

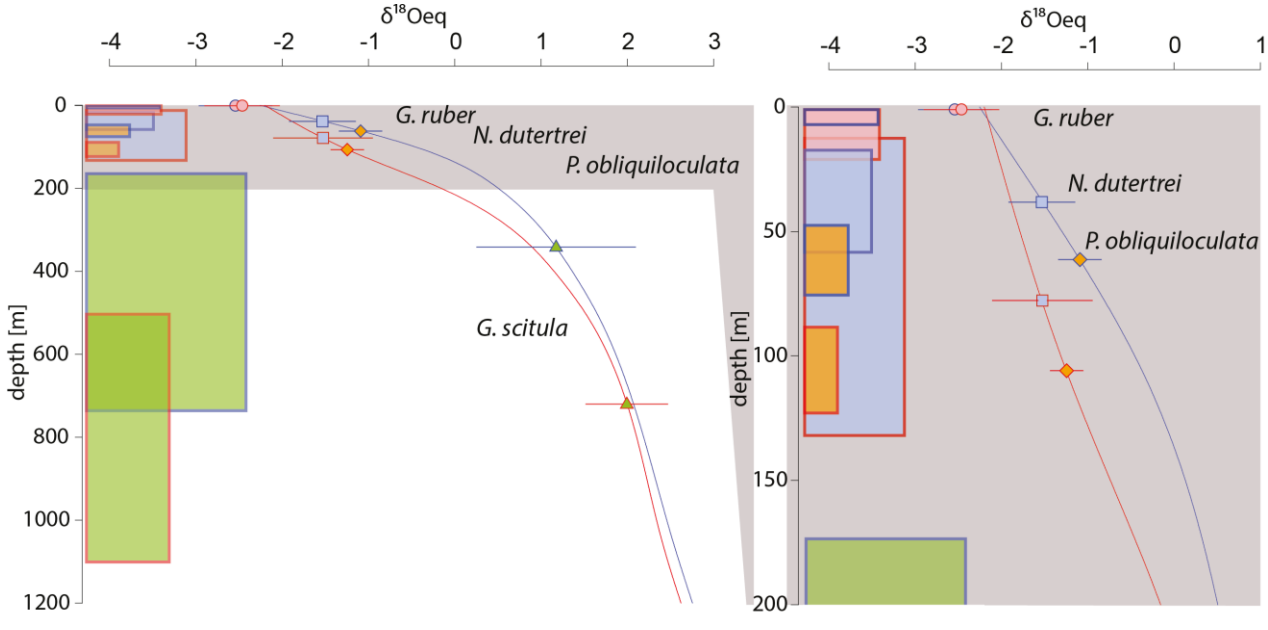

971

972 *Figure 6*

973

a)

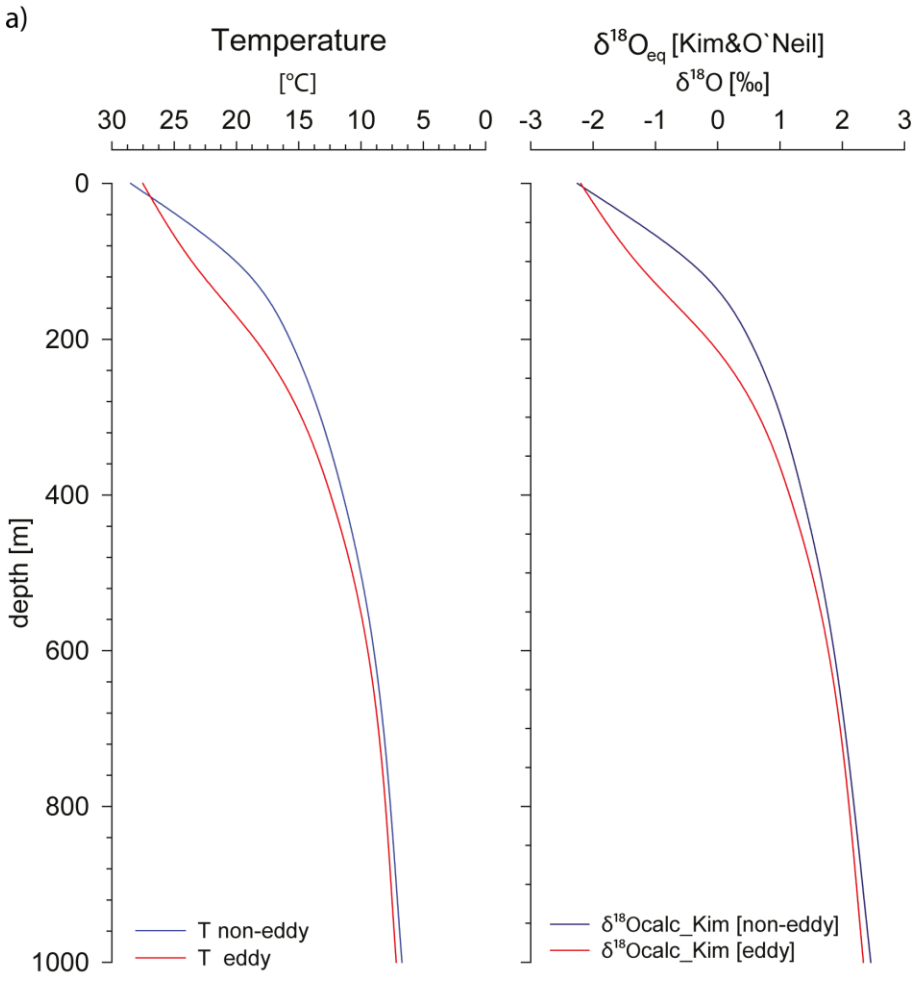
Temperature
[°C]
30 25 20 15 10 5 0
δ18Oeq [Kim&O`Neil]
δ18O [‰]
-3 -2 -1 0 1 2 3
depth [m]
0
200
400
600
800
1000
T non-eddy
T eddy
δ18Ocalc_Kim [non-eddy]
δ18Ocalc_Kim [eddy]

974

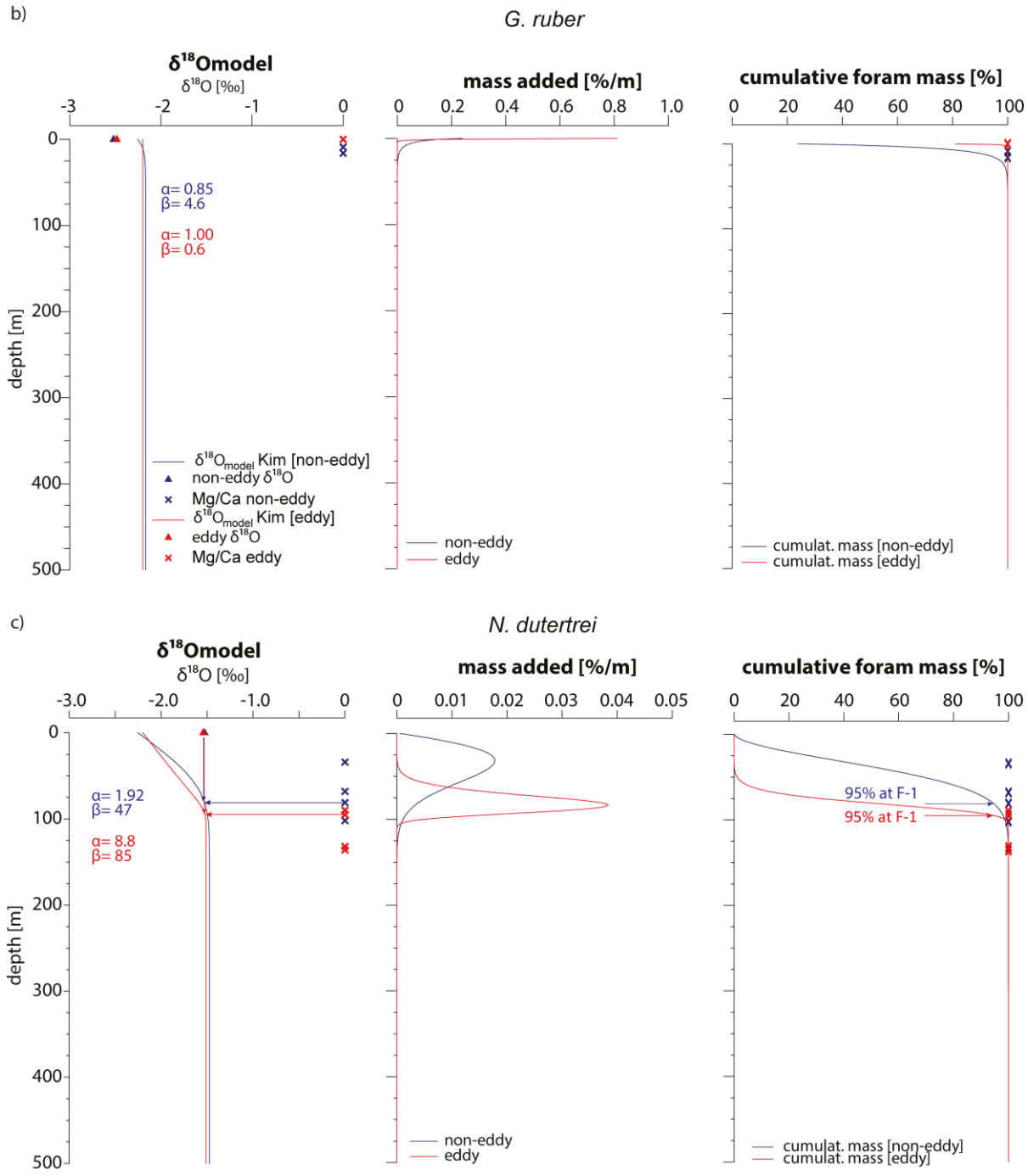
b)
G. ruber
δ18Omodel
δ18O [‰]
-3
-2
-1
0
mass added [%/m]
0
0.2
0.4
0.6
0.8
1.0
cumulative foram mass [%]
0
20
40
60
80
100
depth [m]
0
100
200
300
400
500
α= 0.85
β= 4.6
α= 1.00
β= 0.6
δ18Omodel Kim [non-eddy]
non-eddy δ18O
Mg/Ca non-eddy
δ18Omodel Kim [eddy]
eddy δ18O
Mg/Ca eddy
non-eddy
eddy
cumulat. mass [non-eddy]
cumulat. mass [eddy]
c)
N. dutertrei
δ18Omodel
δ18O [‰]
-3.0
-2.0
-1.0
0
mass added [%/m]
0
0.01
0.02
0.03
0.04
0.05
cumulative foram mass [%]
0
20
40
60
80
100
depth [m]
0
100
200
300
400
500
α= 1.92
β= 47
α= 8.8
β= 85
95% at F-1
95% at F-1
non-eddy
eddy
cumulat. mass [non-eddy]
cumulat. mass [eddy]

975

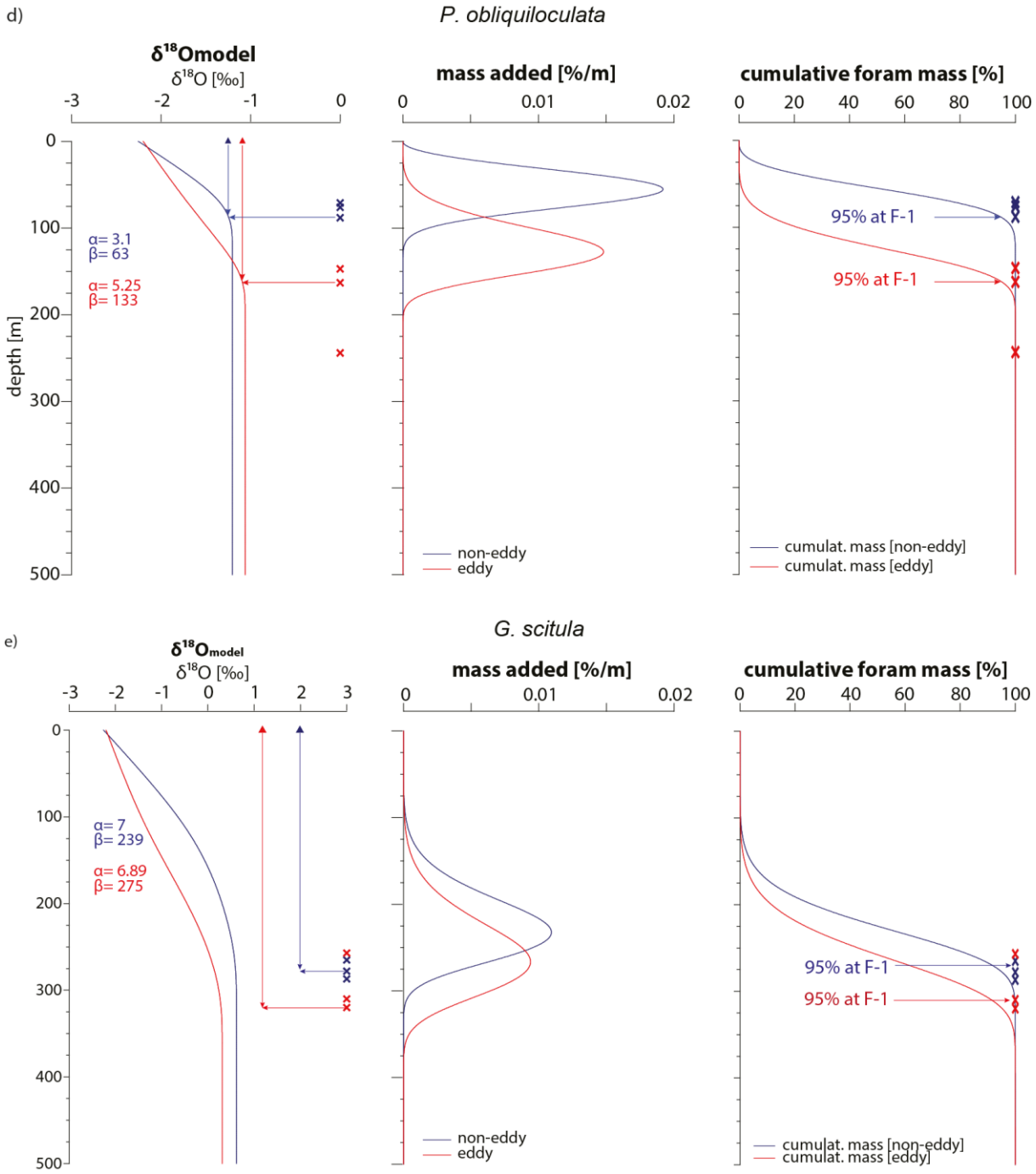

976
977 *Figure 7*

978

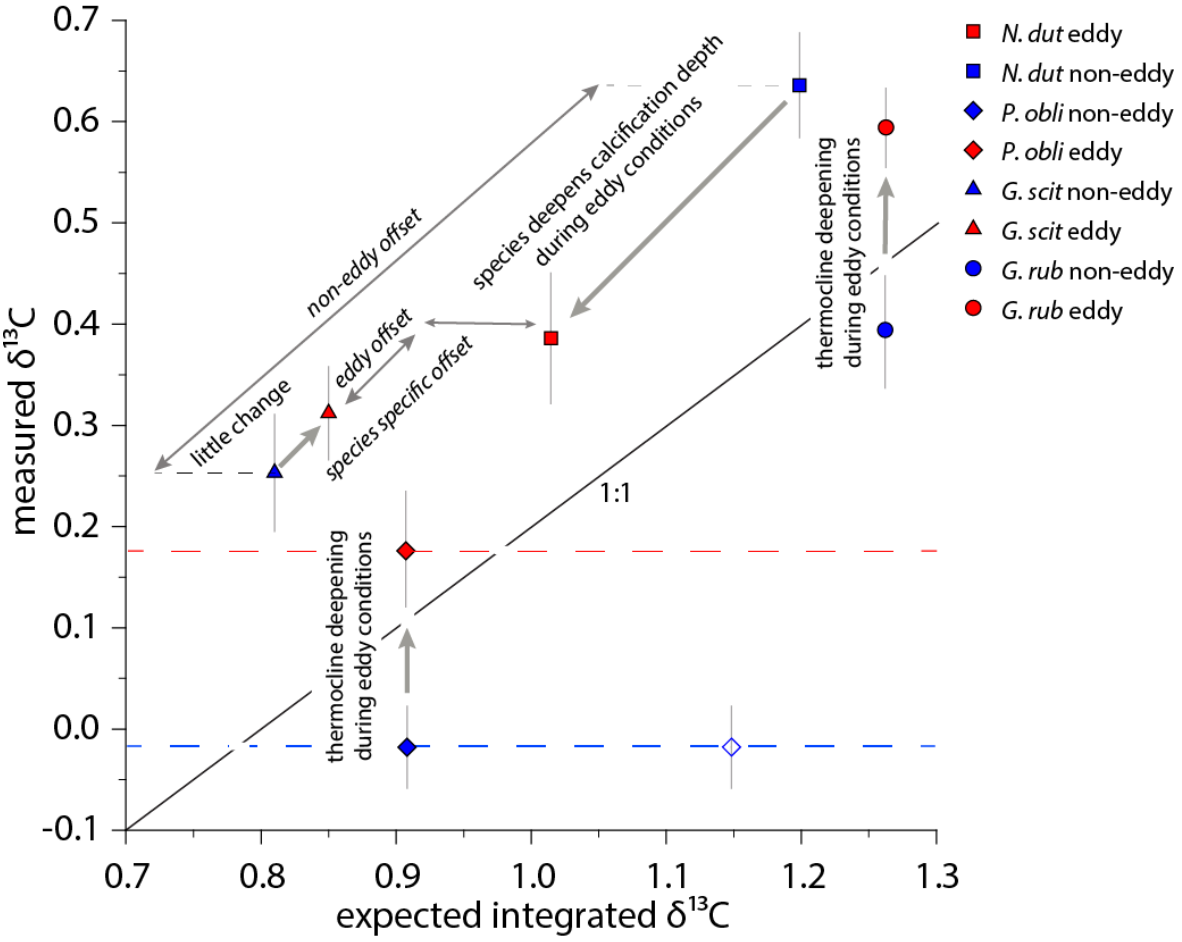

Figure 8

Figure captions:

Figure 1: Hydrography of southwestern Indian Ocean and location of the sediment trap (star) within the mooring array (right top). On the right bottom a map of sea level anomaly shows the passing of an anti-cyclonic eddy over the trap location (star). AVISO sea level anomaly map was produced using the AVISO live access server (http://las.aviso.altimetry.fr/las/getUI.do). EACC: East African Coastal Current, SEC: South Equatorial Current, AC: Agulhas Current.

Table 1: Average Mg/Ca ratios (Steinhardt et al., 2014), $\delta^{18}O$ and $\delta^{13}C$ with standard errors (SE) and corresponding standard deviations (SD). Mg/Ca-based temperature are based on species specific temperature equations. The equation developed by Fallet et al. (2010) was applied for *G. ruber*. The equations developed by Anand et al. (2003) were applied to *N. dutertrei*, *P. obliciloculata*. For *G. scitula* Anand's equation for *G. hirsuta* was applied following the example of Fallet et al. (2011). Calculate $\delta^{18}O$-based temperatures are based on the equation of Kim and O'Neil (1997).

Table 2: Average measurements of $\delta^{18}O$ and $\delta^{13}C$ with standard errors (SE) and corresponding standard deviations (SD) performed at the Universitat Autònoma de Barcelona on a Thermo Finnigan MAT253 mass spectrometer coupled to a Kiel IV device for CO2 sample gas preparation (BCN) and the Thermo Finnigan Delta Plus mass spectrometer equipped with a Gas Bench II preparation device at the VU University Amsterdam (VU). Measurements of *N. dutertrei*, *P. obliquiloculata* and *G. scitula* are comparable and species-specific values are in good agreement

Figure 2: Scatter plot of single shell $\delta^{13}C$ versus $\delta^{18}O$ with analytical error. Note the linear relation in *G. scitula* (r^2=0.388, p<0.001).

Figure 3: Eddy (red circles), non-eddy (blue circles) comparison of $\delta^{13}C$ PDB and $\delta^{18}O$ PDB for the analyzed species. Grey lines indicate standard deviation (SD), black capped lines are indicative of standard error (SE).

Table 3: Results for $\delta^{18}O$ and $\delta^{13}C$ with standard errors (SE) and corresponding standard deviations (SD) under eddy and non-eddy conditions for *G. ruber*, *N. dutertrei*, *P. obliquiloculata* and *G. scitula*.

Figure 4: Scatter plot of Mg/Ca versus $\delta^{18}Occ$ (left panel). Right panel: single chamber Mg/Ca exponential relationship with $\delta^{18}O$-derived Temperatures calculated using Kim & O'Neil (1997). Regression: f = a*exp(b*x), with a=-0.7, b=0.06, r^2=0.47 using F-1/2 Mg/Ca from *G. ruber*, F-0 for *N. dutertrei*, *P. obliquiloculata* and *G. scitula* (black circles). F-1 for *N. dutertrei*, *P. obliquiloculata* and *G. scitula* (red circles) and F-2 for *N. dutertrei, P. obliquiloculata* and *G. scitula* (blue circles). Mg/Ca data from Steinhardt et al. (2014). Note that the correlation coefficient also indicates that approximately 60% of the observed variability is not due to temperature alone.

Figure 5: Inter-species $\delta^{18}O$- and Mg/Ca-derived temperature for eddy and non-eddy intervals. Circles: $\delta^{18}O$-based temperatures using the equation of Kim and O'Neil (1997), Squares represent Mg/Ca-based temperatures using the species specific equations of Anand et al. (2003) for *N. dutertrei*, *P. obliquiloculata* and *G. scitula*. For *G. ruber*, the equation of Fallet et al. (2011) was used. Vertical error bars (SD) for $\delta^{18}O$ derived temperatures, horizontal error bars (SD) for Mg/Ca derived temperatures. Red colors: *G. ruber*, blue: *N dutertrei*, orange: *P. obliquiloculata*, green: *G. scitula*.

Figure 6: Apparent calcification depths of species are generally shallower during non-eddy conditions. Apparent calcification depths for eddy (red) and non-eddy conditions (blue) calculated from single specimen $\delta^{18}O_{cc}$ using *in situ* temperature and $\delta^{18}O_{w.}$ Calcification depth was determined by matching the measured foraminiferal $\delta^{18}O_{cc}$ with the $\delta^{18}O_{eq}$, using the equation of Kim and O'Neil (1997). We used $\delta^{18}O_{SW}$ from the species calcification depth. Grey box indicates the zone of the close-up on the right (upper 200 m).

Figure 7: Cumulative calcification model for eddy (red) and non-eddy (blue) conditions from left to right: temperature profiles as well as $\delta^{18}O_{equilibrium}$ ($\delta^{18}O_{eq)}$ for the upper 1000 m and $\delta^{18}O_{cummulative}$ ($\delta^{18}O_{model}$) for the upper 500m (a). On the upper far right, mass development/growth pattern, below cumulative mass of the foraminifera (foram mass) is plotted for the upper 500 m. Bulk $\delta^{18}O_{foram}$

(triangles) Mg/Ca derived single chamber calcification depth (crosses) are indicated in the relevant plots for *G. ruber* (b), *N. dutertrei* (c), *P. obliquiloculata* (c) and *G. scitula* (d)

Figure 8: Inter-species differences between expected $\delta^{13}C$ values, based on the cumulative mass balance model, and measured $\delta^{13}C$ values of *G. ruber*, *N. dutertrei, P. obliquiloculata* and *G. scitula*. Dashed line indicates the 1:1 line of measured and expected $\delta^{13}C$. Red symbols represent values for eddy conditions, blue symbols represent values for non-eddy condition. Thick grey arrows indicate intra-species trends between non-eddy and eddy conditions, thin arrows indicate inter-specific trends. *P. obliquiloculata* does not calcify in isotopic equilibrium with dissolved $\sum CO_2$, but the deviation from isotopic equilibrium is a linear function of temperature (Mulitza et al., 1999), hence there is no projected $\delta^{13}C_{exect}$, this is indicated by the dotted lines. Open diamond indicates $\delta^{13}C_{exect}$ for *P. obliquiloculata* non-eddy conditions.